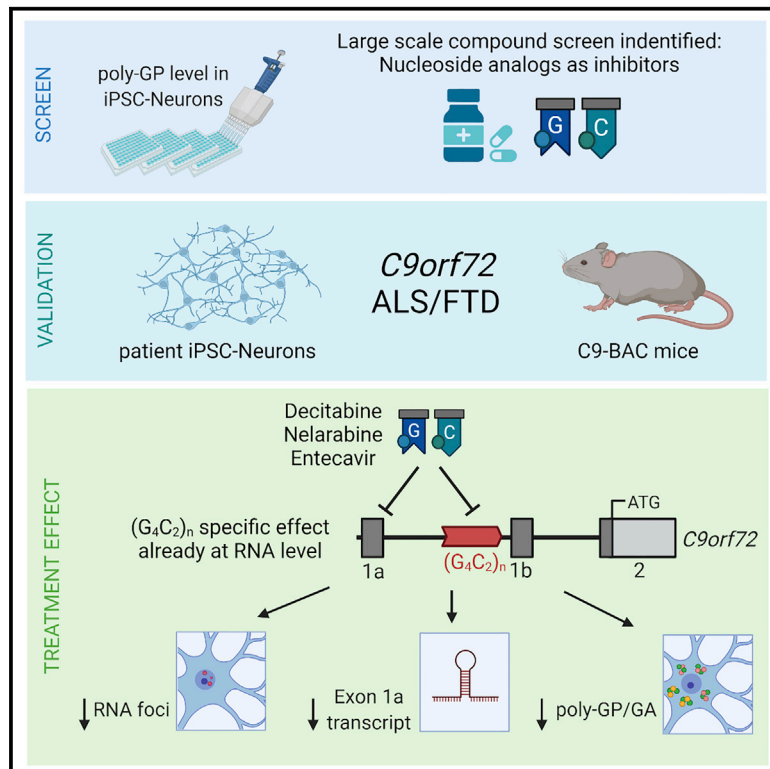# Drug screen in iPSC-Neurons identifies nucleoside analogs as inhibitors of $(G_4C_2)_n$ expression in *C9orf72* ALS/FTD

Graphical abstract

Authors

Mareike Czuppa, Ashutosh Dhingra, Qihui Zhou, ..., Patrizia Rizzu, Peter Heutink, Dieter Edbauer

Correspondence

ashutosh.dhingra@dzne.de (A.D.), dieter.edbauer@dzne.de (D.E.)

In brief

Screening 1,430 approved drugs in patient-derived iPSC-Neurons for inhibitors of dipeptide repeat (DPR) expression in *C9orf72* ALS/FTD, Czuppa et al. identify three nucleoside analogs: decitabine, nelarabine, and entecavir. The compounds nearly abolish foci of the $(G_4C_2)_n$ repeat RNA without affecting global gene expression. The findings are validated in transgenic mice.

Highlights

- Screen for DPR modifiers in *C9orf72* iPSC-Neurons yields guanosine/cytidine analogs

- Decitabine, entecavir, and nelarabine reduce expression of repeat RNA and DPR levels

- Decitabine does not act via DNMT and has minimal effects on transcriptome

- Decitabine is most potent *in vitro* and reduces pathology in a *C9orf72* mouse model

CellPress

Cell Reports

Report

Drug screen in iPSC-Neurons identifies nucleoside analogs as inhibitors of $(G_4C_2)_n$ expression in *C9orf72* ALS/FTD

Mareike Czuppa,[1,9] Ashutosh Dhingra,[2,9,*] Qihui Zhou,[1,3,9] Carina Schludi,[1] Laura König,[1] Elisabeth Scharf,[1] Daniel Farny,[1] Anupriya Dalmia,[2] Joachim Täger,[2] Melissa Castillo-Lizardo,[2] Eszter Katona,[1] Kohji Mori,[4] Tina Aumer,[5] Florian Schelter,[5] Markus Müller,[5] Thomas Carell,[5] Tuomo Kalliokoski,[6] Josef Messinger,[6] Patrizia Rizzu,[2] Peter Heutink,[2,7] and Dieter Edbauer[1,3,8,10,*]

[1]German Center for Neurodegenerative Diseases (DZNE), Munich, Germany
[2]German Center for Neurodegenerative Diseases (DZNE), Tübingen, Germany
[3]Munich Cluster for Systems Neurology (SyNergy), Munich, Germany
[4]Psychiatry, Graduate School of Medicine, Osaka University, Suita, Japan
[5]Ludwig-Maximilians-University Munich, Faculty of Chemistry and Pharmacy, Munich, Germany
[6]Orion Corporation Orion Pharma, Medicine Design, Espoo, Finland
[7]Hertie Institute for Clinical Brain Research, University of Tübingen, Tübingen, Germany
[8]Ludwig-Maximilians-University Munich, Graduate School of Systemic Neurosciences (GSN), Munich, Germany
[9]These authors contributed equally
[10]Lead contact
*Correspondence: ashutosh.dhingra@dzne.de (A.D.), dieter.edbauer@dzne.de (D.E.)
https://doi.org/10.1016/j.celrep.2022.110913

SUMMARY

An intronic $(G_4C_2)_n$ expansion in *C9orf72* causes amyotrophic lateral sclerosis and frontotemporal dementia primarily through gain-of-function mechanisms: the accumulation of sense and antisense repeat RNA foci and dipeptide repeat (DPR) proteins (poly-GA/GP/GR/PA/PR) translated from repeat RNA. To therapeutically block this pathway, we screen a library of 1,430 approved drugs and known bioactive compounds in patient-derived induced pluripotent stem cell-derived neurons (iPSC-Neurons) for inhibitors of DPR expression. The clinically used guanosine/cytidine analogs decitabine, entecavir, and nelarabine reduce poly-GA/GP expression, with decitabine being the most potent. Hit compounds nearly abolish sense and antisense RNA foci and reduce expression of the repeat-containing nascent *C9orf72* RNA transcript and its mature mRNA with minimal effects on global gene expression, suggesting that they specifically act on repeat transcription. Importantly, decitabine treatment reduces $(G_4C_2)_n$ foci and DPRs in *C9orf72* BAC transgenic mice. Our findings suggest that nucleoside analogs are a promising compound class for therapeutic development in *C9orf72* repeat-expansion-associated disorders.

INTRODUCTION

Repeat expansions in multiple genes cause a wide range of neurodegenerative diseases by altering gene expression and causing RNA or protein toxicity (Rodriguez and Todd, 2019; Swinnen et al., 2020). The relative role of these components is hard to dissect experimentally, and synergistic effects are likely. About 10% of all patients suffering from amyotrophic lateral sclerosis (ALS) and frontotemporal dementia (FTD) carry a pathogenic $(G_4C_2)_n$ repeat expansion in a non-coding region between the two alternative first exons of *C9orf72* (DeJesus-Hernandez et al., 2011; Gijselinck et al., 2012; Renton et al., 2011). The repeat RNA is transcribed within the first intron of a low-abundance transcript variant starting at the upstream exon. Additionally, an antisense $(C_4G_2)_n$ transcript is found in the disease. Sense and antisense repeat transcripts accumulate in nuclear RNA foci and can partially sequester several

RNA-binding proteins (Cooper-Knock et al., 2014; DeJesus-Hernandez et al., 2011; Donnelly et al., 2013). The sense transcript of the $(G_4C_2)_n$ repeat is translated into abundant dipeptide repeat (DPR) proteins poly-GA, -GP, and -GR by a non-canonical mechanism called repeat-associated non-ATG (RAN) translation (Ash et al., 2013; Mori et al., 2013b; Zu et al., 2011, 2013). The antisense transcript $(C_4G_2)_n$ yields rare poly-PA, -PR, and additional -GP via the same mechanism (Gendron et al., 2013; Mori et al., 2013a; Zu et al., 2013). Non-canonical initiation may occur through a permissive structure directly within the repeat RNA or near-cognate start codons (e.g., CTG) upstream of the repeat and may further involve frameshifting (Almeida et al., 2019; Green et al., 2017; McEachin et al., 2020; Tabet et al., 2018). Overexpression of the $(G_4C_2)_n$ repeat or recombinant poly-GA/GR/PR in animal models causing neuron loss argues for predominant gain-of-function pathomechanisms through RNA and/or protein toxicity (Chew

et al., 2015; Jiang et al., 2016; LaClair et al., 2020; Mizielinska et al., 2014).

Since specific therapies for *C9orf72* ALS/FTD are still lacking, multiple groups have focused on identifying binders for repeat RNA or inhibitors of RAN translation. Intrathecal delivery of antisense oligonucleotides (ASOs) targeting the sense transcript is currently in clinical trials, based on encouraging preclinical studies that showed robust reduction of RNA foci and DPR expression in mice (Jiang et al., 2016). Moreover, inhibiting protein kinase R and high-dose metformin showed a promising reduction of RAN translation in cells and mice without affecting RNA levels (Zu et al., 2020). Several groups developed novel compounds preferentially binding the G-quadruplex or hairpin conformation of $(G_4C_2)_n$ RNA *in vitro*, since these structures may regulate RAN translation or sequestration of RNA-binding proteins (Simone et al., 2018; Su et al., 2014; Wang et al., 2019). Others used an *in vitro* translation assay to identify small molecules preferentially reducing non-ATG repeat translation, but the compounds showed incomplete selectivity over global translation, limiting their therapeutic application (Green et al., 2019).

To identify alternative treatment mechanisms and compounds that could be repurposed for *C9orf72* ALS/FTD, we phenotypically screened a library of FDA-approved drugs for modifiers of DPR expression in induced pluripotent stem cell-derived neurons (iPSC-Neurons) from patients with *C9orf72* that contain the full-length repeat expansion and express endogenous DPRs and RNA foci. Notably, we identified three guanosine/cytidine analogs clinically used for the therapy of cancer and viral diseases that reduced DPR expression similar to an ASO targeting the repeat-containing *C9orf72* intron. Further analysis of poly-GA levels, RNA foci, *C9orf72* transcript isoforms and reporter constructs suggests that the compounds target the core *C9orf72* pathomechanisms already at the level of repeat transcription or stability without directly binding to the repeat RNA or interfering with non-canonical or global translation. We validated the effects of the most potent compound, decitabine, in a proof-of-concept study in *C9orf72* BAC mice.

RESULTS

Phenotypic screening identifies decitabine, nelarabine, and entecavir as inhibitors and ralimetinib as an enhancer of poly-GP expression

To generate patient-derived neurons for large-scale compound screening, we adapted a protocol using doxycycline-inducible expression of NGN2 in a neuronal precursor intermediate state (Busskamp et al., 2014; Dhingra et al., 2020; Zhang et al., 2013). We confirmed differentiation into upper-layer cortical neurons and *C9orf72*-specific expression of both sense and antisense RNA foci as well as poly-GP measured by immunoassay (Figures S1A–S1D) (Lehmer et al., 2017). A validated ASO targeting the repeat-containing intron 1 of *C9orf72* (Jiang et al., 2016) significantly reduced endogenous poly-GP within 7 to 9 days, which is consistent with the long half-life established for over-expressed DPRs (Westergard et al., 2019) (Figure S1E). Therefore, we chose a 9-day protocol with two consecutive drug applica-

tions and the targeting ASO as a positive control to screen for modifiers of poly-GP expression (Figure S1F).

In total, we screened 1,430 compounds at 10 μM in 6 replica plates, each containing four solvent controls for normalization and three negative and three positive ASO controls randomly distributed on the plate (Table S1). The relationship between effects on poly-GP and total protein levels for all samples was plotted on a scatterplot, which revealed clustering of ASO controls and some outliers with low protein concentration (Figure 1A). Histograms show bimodal distribution of poly-GP and total protein levels, which likely reflects true toxicity as well as occasional detachment of the whole cell layer during plate handling observed by automated bright-field microscopy. Thus, we excluded all replicates with less than 75% mean protein level compared with solvent controls to select promising primary hits with low toxicity. This approach yielded four enhancers (Hsp90 inhibitor tanespimycin, Bcr-Abl inhibitor dasatinib, antihistaminic cyproheptadine, and p38 inhibitor ralimetinib) and three inhibitors (antiviral entecavir and cancer drugs decitabine and nelarabine) with more than 20% effect on poly-GP expression (Figure 1B). While the filtered enhancers did not show apparent commonalities, the three inhibitors all belong to the group of guanosine/cytidine analogs. Thirty-four other nucleoside analogs including 16 other guanosine/cytidine analogs from the compound library did not affect poly-GP levels or were toxic at 10 μM (Table S2).

Next, we analyzed the dose response for each hit compound using the same treatment protocol. We replicated upregulation of poly-GP by tanespimycin, dasatinib, and ralimetinib at 10 μM (Figure S2A). Dasatinib, tanespimycin, and cyproheptadine were excluded from further analysis due to onset of toxicity. The effect of ralimetinib was replicated in iPSC-Neurons from three additional patients (Figure S2C). The high concentration (10 μM) of ralimetinib required to increase DPR expression does not fit its IC_{50} for p38 MAP kinase (10–40 nM), suggesting that other low-affinity targets may exist (Lin et al., 2019).

The three guanosine/cytidine analogs consistently reduced poly-GP levels in iPSC-Neurons derived from four different patients, including one unusual case with only 70 repeats (Figure 1C, light blue). The antiviral entecavir, the cytostatic nelarabine, and the DNA methyl-transferase (DNMT) inhibitor decitabine reduced poly-GP levels with an IC_{50} of 3.29, 0.22, and 0.054 μM, respectively. Based on total protein levels (Figure S2B), tubulin staining (Figure 1D), and LIVE/DEAD staining (Figure S3A), toxicity was negligible in post-mitotic neurons up to 10 μM. Therefore, decitabine and other guanosine/cytidine analogs are promising inhibitors of poly-GP expression from the $(G_4C_2)_n$ repeat in *C9orf72*.

Nucleoside analogs also reduce poly-GA but do not act on RAN translation or through DNMT inhibition

Decitabine is known to be incorporated into genomic DNA during replication, which in turn inhibits DNMT (Oz et al., 2014). However, other nucleoside (5-Fluoro-2′-deoxycytidine; FdCyd) and non-nucleoside (RG108) DNMT inhibitors did not affect poly-GP expression up to 100 μM (Figure S3B). Analyzing global DNA methylation using mass spectrometry
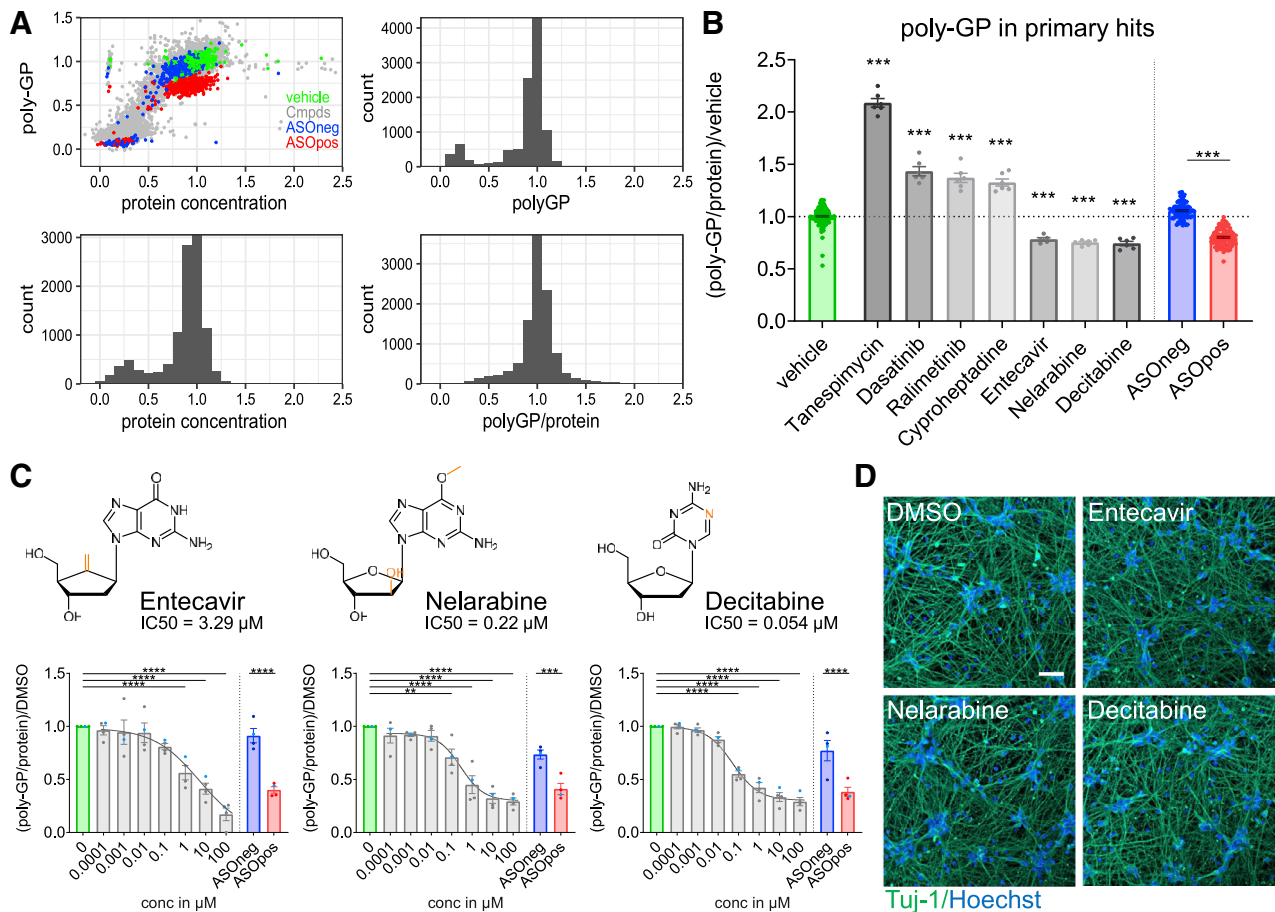
Figure 1. Screening 1,430 approved drugs in iPSC-Neurons yield three nucleoside analogs as inhibitors of poly-GP expression

iPSC-Neurons were treated with 10 μM compounds or 2 μM ASO on days 3 and 8 of differentiation and analyzed on day 12 (Figure S1F).

(A) Data from all 10,614 wells from compound screen. Scatterplot of poly-GP and protein levels normalized to the 4 vehicle control wells within each plate. Histograms of absolute and relative poly-GP and protein levels.

(B) Selection of compounds showing at least 20% modulation of poly-GP levels with less than 25% reduction in total protein for at least 3 of 6 replicates. Poly-GP levels are normalized to total protein levels and the within-plate vehicle control. Vehicle n = 152 (146 DMSO, 6 water), ASOneg: n = 83 and ASOpos: n = 96 were pooled from plates containing hit compounds; Entecavir: n = 5, others: n = 6.

(C) Nucleoside analogs show clear reduction of normalized poly-GP levels in a concentration-dependent manner in iPSC-Neurons from n = 4 different patients with *C9orf72*. All data are normalized to DMSO control within patients (6 technical replicates). Light blue dots denote data from 70-repeat line. Overlay shows fit for dose-response curve. Chemical structures of the analogs with modifications highlighted in orange. Raw data for the screening line is shown in Figure S2B. Enhancers are validated in Figure S2A.

(D) Immunofluorescence staining of iPSC-Neurons with neuronal marker Tuj-1 (green) and nuclear marker Hoechst (blue) shows no toxicity of inhibitors (10 μM) compared with vehicle. Scale bar: 50 μm.

Statistics for (B) and (C): bar graphs show mean with SEM; (B): Kruskal-Wallis test and subsequent pairwise Wilcoxon rank sum tests; and (C): pairwise t test, both with Benjamini-Hochberg correction for comparison of key groups: $****p < 0.0001$, $***p < 0.001$.

(MS) did not show changes upon decitabine treatment (Figure S3C), suggesting that it lowers poly-GP through a different mechanism.

Next, we tested whether the lead compounds also affect poly-GA expression in iPSC-Neurons. Indeed, the nucleoside analogs also reduced poly-GA, while the alternative DNMT inhibitor FdCyd had no effect and ralimetinib increased poly-GA levels. Normalizing DPR levels to endogenous tau levels showed a similar reduction of poly-GA/GP by nucleoside analogs, suggesting that the effects are not due to the downregulation of global translation (Figures 2A and S3D).

To test whether the nucleoside analogs act specifically on the non-ATG-mediated translation of $(G_4C_2)_n$ repeats or also affect canonical $(G_4C_2)_n$ translation, we transduced rat primary cortical neurons with two constructs containing either the endogenous TAG stop codon in the poly-GP frame directly upstream of the $(G_4C_2)_n$ repeat or an artificial ATG start codon (Figure 2B). Nelarabine and decitabine inhibited poly-GA/GP expression also in the presence of an ATG start codon, suggesting that the compounds do not exclusively act on RAN translation. Interestingly, we noted a mild reduction of the $(G_4C_2)_n$ transcript (Figure 2B). Moreover, decitabine reduced
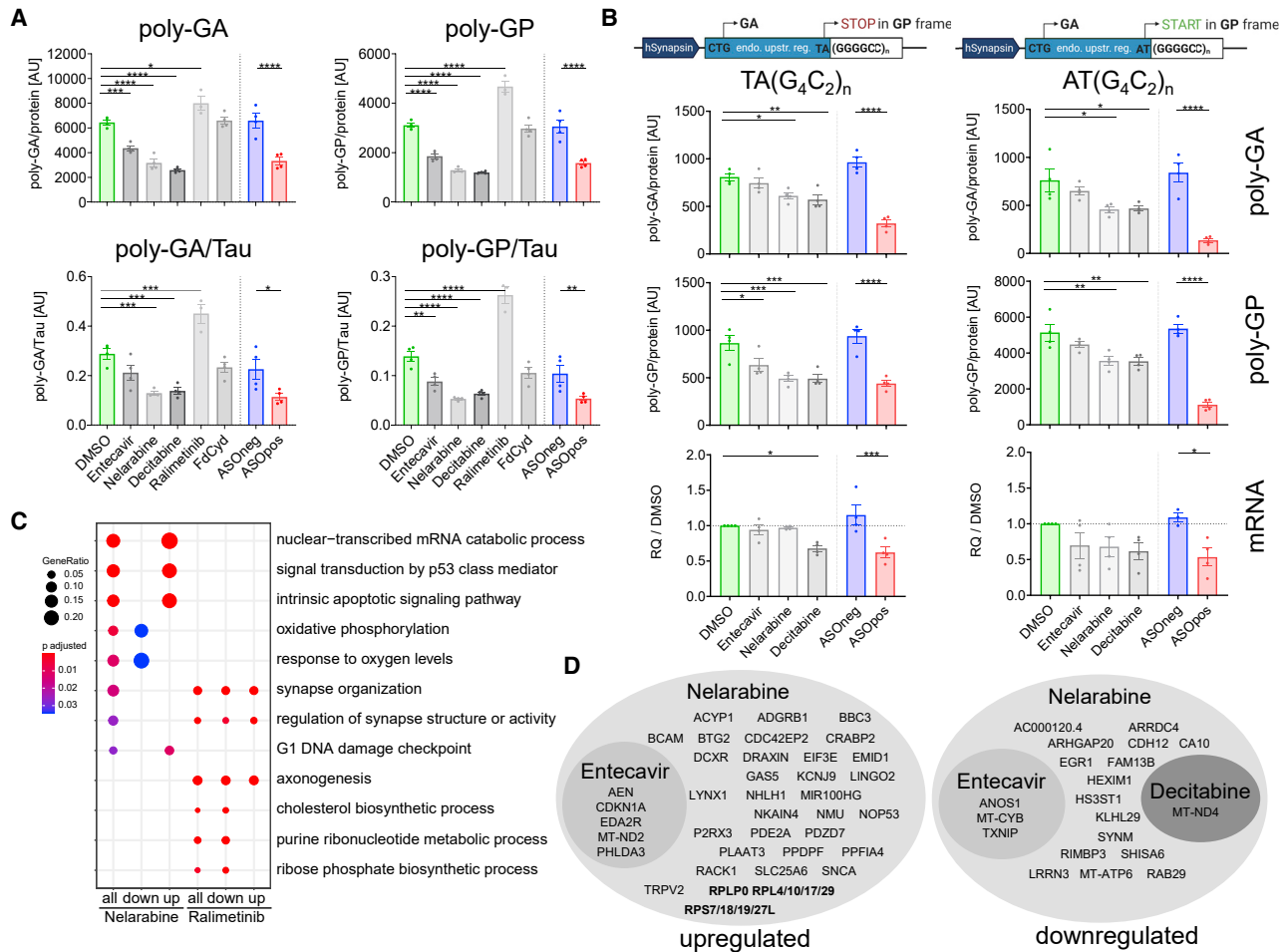
Figure 2. Nucleoside analogs reduce expression of DPR proteins without affecting RAN translation

(A) *C9orf72* iPSC-Neurons treated with selected hit compounds and DNMT inhibitor 5-Fluoro-2'deoxycytidine (FdCyd), (10 μM) or ASOs (2 μM). Poly-GA/GP levels were normalized to total protein or tau levels (n = 4). Raw data are shown in Figure S3D.

(B) Rat primary neurons transduced with the depicted $(G_4C_2)_n$ constructs were treated with indicated compounds (transduction on days *in vitro* [DIV]6, treatment [10 μM] on DIV7, harvest on DIV10). Poly-GA/GP levels were normalized to total protein. Relative expression (RQ) of the reporter mRNA; n = 6. Antisense reporter shown in Figure S3E.

(C) RNA-seq analysis of *C9orf72* iPSC-Neurons treated as in (A) and subsequent Gene Ontology analysis of regulated genes shows upregulation of translation and p53 response by nelarabine and widespread expression changes of synaptic genes by ralimetinib. Full dataset in Table S3A.

(D) Differentially expressed genes overlap between cells treated with nelarabine, entecavir, and decitabine. All transcripts passing multiple testing correction are shown. Full dataset in Table S3B.

Statistical analysis for (A) and (B): bar graphs show mean with SEM, ordinary one-way ANOVA with Sidak's multiple comparison post-test: ****$p < 0.0001$, ***$p < 0.001$, **$p < 0.01$, *$p < 0.05$.

poly-GP translated from an antisense reporter construct (Figure S3E).

Next, we analyzed RNA incorporation of decitabine using *in vitro* transcription of a $(G_4C_2)_n$ construct using T7 RNA polymerase. Adding up to 20 mM decitabine triphosphate to the reaction did not affect the resulting RNA levels and the subsequent translation assay (Figure S3F). We were not able to detect incorporation of decitabine into the $(G_4C_2)_n$ transcript using established MS protocols (Traube et al., 2019). Importantly, global incorporation of decitabine into RNA from iPSC-Neurons (after 1, 4, or 9 days of treatment) could be ruled out as well (data not shown). Moreover, we did not detect binding of the three in-

hibitors to $(G_4C_2)_{10}$ RNA in G-quadruplex or hairpin conformation by surface plasmon resonance assay at 50 μM *in vitro* (see STAR Methods).

To investigate the mode of action and potential side effects, we analyzed differential gene expression in post-mitotic *C9orf72* iPSC-Neurons by RNA sequencing (RNA-seq). Our data showed modest expression changes in decitabine (1 gene), entecavir (8 genes), or nelarabine (64 genes) treated neurons compared with the solvent control and no significant changes upon FdCyd treatment (Table S3B). Nelarabine increased the levels of several ribosomal components and p53 target genes such as CDKN1A/p21 and decreased the

expression of some mitochondrial genes (Figures 2C and 2D). Interestingly, all transcripts affected by entecavir or decitabine were concordantly regulated by nelarabine (Figure 2D). The enhancer ralimetinib significantly affected 1,511 genes mainly implicated in synaptic function (Figure 2C; Table S3A), which may explain increased DPR levels due to enhanced synaptic activity (Westergard et al., 2019). The effects of the hit compounds on DPR expression cannot be attributed to global dysregulation of GC-rich transcripts (Figure S3G), and the minimal effects on global RNA expression excluded major side effects in neurons.

To address potential beneficial effects on *C9orf72* specific toxicity, we investigated the levels of previously reported disease-signature genes *NEDD4L*, *FAM3C2*, *CHRDL1*, *SERPINE2*, and *SEPP1/SELENOP* (Donnelly et al., 2013), but even without multiple-testing correction, we found no significant expression changes (Table S3B). Moreover, *C9orf72* ASO did not significantly affect these (or any other) genes, suggesting that under our acute culture conditions, *C9orf72* iPSC-Neurons do not express a disease signature (Table S3C).

Nucleoside analogs inhibit transcription of $(G_4C_2)_n$ RNA resulting in long-lasting suppression of RNA foci and poly-GA/GP

Since our findings so far suggest nucleoside analogs act upstream of translation, we focused on examining their effects on the RNA level in iPSC-Neurons from three *C9orf72* mutation carriers. Fluorescence *in situ* hybridizations (FISHs) and subsequent automated image analysis revealed a striking reduction of sense RNA foci that even exceeded the effects of the ASO positive control after 9 days of treatment (Figures 3A and 3B). Ralimetinib had no significant effect on RNA foci, suggesting it induces DPR expression through a distinct pathway.

To test whether the effects on RNA foci are due to altered mRNA expression, we analyzed the key *C9orf72* isoforms by quantitative RT-PCR. Entecavir, nelarabine, decitabine, and the ASO targeting the first intron mainly affected transcripts starting from exon 1a, which harbors the $(G_4C_2)_n$ repeat in the first intron of the pre-mRNA (Figures 3C and 3D). Importantly, the nucleoside analogs did not alter *C9orf72* exon 1a and 1b expression in control iPSC-Neurons without $(G_4C_2)_n$ expansion, suggesting that the compounds act only on the primary transcript containing the expanded repeat (Figure S3H).

To analyze transcription directly, we measured nascent exon 1a RNA using pre-mRNA-specific primers in a 5-ethynyl uridine (EU) incorporation assay, biotin azide labeling, and subsequent pull down using translational inhibitor actinomycin as positive control. Interestingly, decitabine treatment led to strong reduction of nascent exon 1a transcripts (Figure S4A), suggesting an effect on repeat-specific transcription.

Due to potential indirect effects on transcription, we investigated DNA-repair mechanisms, although the hit compounds did not induce major DNA damage in primary neurons as measured by γ-H2A.X immunofluorescence (Figure S4B). Next, we used knockdown experiments to test whether the DNA-repair machinery is required for activity of the nucleoside analogs. siRNAs against key components of the DNA mismatch repair (*MLH1*, *PMS1/MLH2*, *PMS2/MLH4*, *MSH2*), nucleotide excision repair (*XPA*, *ERCC3/XPB*, *XPC*), base ex-

cisions repair (*FEN1*), and non-homologous end-joining (*XRCC6/Ku70*) did not reduce basal poly-GP levels or alter decitabine-induced suppression of poly-GP in *C9orf72* iPSC-Neurons (Figures S4C and S4D).

Since drug-induced repeat contractions have been shown for $(CAG)_n$ expansions (Nakamori et al., 2020), we analyzed the repeat length in *C9orf72* iPSC-Neurons treated with nucleoside analogs using a commercial assay able to precisely measure up to 149 repeats (Figure S4E). However, none of the compounds altered the pattern, which strongly argues against functionally relevant repeat contraction because poly-GP expression is sensitive to nucleoside analogs even in the 70-repeat iPSC-Neuron line (Figures 1C and S2C).

Next, we tested the effect of the compounds in time course experiments. We noticed prominent suppression of $(G_4C_2)_n$ RNA sense foci already after 4 days and delayed reduction of antisense foci after 15–20 days of treatment (Figure 3E). Presumably due to their long half-life, both poly-GP and -GA levels kept dropping with continuous treatment for 20 days in the absence of noticeable toxicity, suggesting that chronic treatment is well tolerated and could be even more beneficial.

We also tested how long the effects would last upon wash out of the compounds after two consecutive treatments (Figure 3F). The exon 1a transcript levels (Figures 3A and 3E) recovered already after 2 days, while sense RNA foci and poly-GA/GP remained low for at least 5 days and only slightly increased after 10 days wash out compared with ASO treatment (Figure 3F).

Taken together, nucleoside analogs act on repeat transcriptions, without invoking DNA-repair mechanisms or repeat contraction, despite long-lasting suppression of poly-GA/GP expression.

Decitabine reduces $(G_4C_2)_n$ RNA and DPRs in *C9orf72* BAC mice

To validate our findings *in vivo*, we treated 9-month-old C9[19] BAC mice (Jiang et al., 2016) with high-dose decitabine for 7 days. We administered 0.6 mg/kg decitabine daily through intraperitoneal (i.p.) injection, which was well tolerated with mild weight loss. The treatment significantly reduced the number of sense foci in the hippocampus within 7 days compared with mice treated with PBS (Figure 4A). Slight reduction of antisense foci did not reach significance within 7 days of treatment, consistent with our *in vitro* data (Figure 3E). Expression of the exon 1a transcript variant was strongly reduced both in the hippocampus and neocortex, while the exon 1b variant was spared (Figure 4B). In addition, we measured DPR levels in soluble and insoluble fractions of the neocortex. Poly-GA reduction was most pronounced for soluble, but was also detectable for the more "mature" insoluble, poly-GA. For poly-GP (~90% soluble), we noticed a clear trend toward reduction, which did not reach statistical significance (Figure 4C). Taken together, the *in vitro* effects of decitabine were replicated in a *C9orf72* BAC mouse model.

DISCUSSION

Nucleoside analogs designed to be incorporated into human or viral DNA have a long history as therapy for cancer and viral
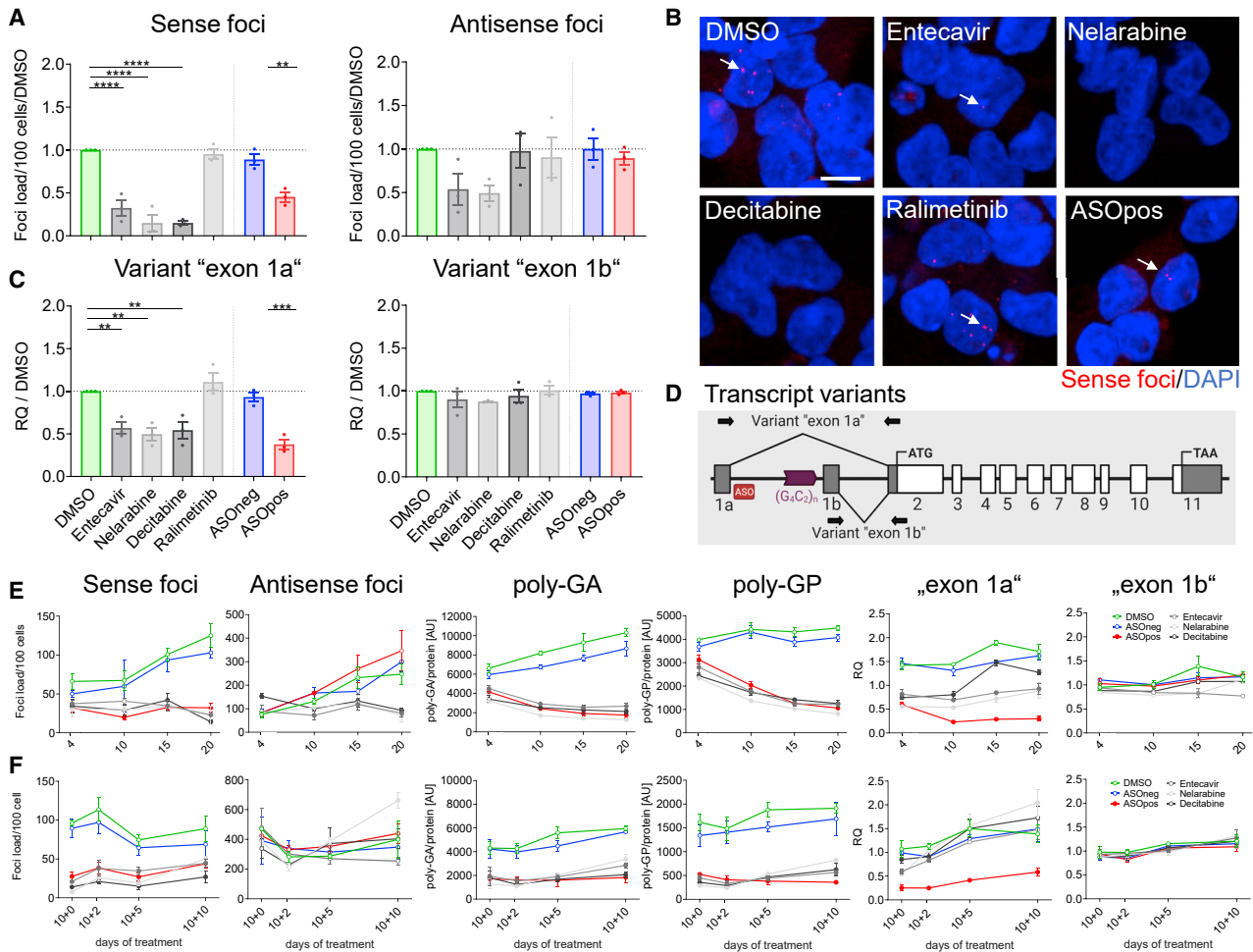
Figure 3. Nucleoside analogs inhibit DPR expression on the RNA level resulting in long-lasting suppression of foci and DPRs

iPSC-Neurons were treated with compounds (10 μM) as in Figure 1 or for time course experiments as indicated.

(A) Sense and antisense nuclear foci were stained with FISH in neurons from n = 3 iPSC lines and automatically quantified. The foci load was normalized to DMSO control within each line (3 technical replicates each, with on average 696 neurons).

(B) Representative FISH images. Sense RNA foci in red and nuclear staining with DAPI in blue. White arrows mark typical foci. Scale bar: 10 μm.

(C) *C9orf72* mRNA was quantified by qRT-PCR using primers amplifying two specific transcript variants as depicted in the schematic diagram in (D). Nucleoside analogs and the intron-targeting ASO positive control specifically repress the transcript starting at exon 1a containing the $(G_4C_2)_n$ in its pre-mRNA. n = 3 different *C9orf72* lines as in (B). Compare Figure S3C for mRNA expression in control lines.

(D) Schematic diagram of qPCR primers and ASO positive control targeting different *C9orf72* transcripts, variants exon 1a and exon 1b, containing or lacking the intronic $(G_4C_2)_n$ repeat. Note that the repeat region is spliced out in the mature mRNA.

(E) Time course experiment (10 μM fresh compound added during media changes on days 3, 8, 13, and 18 of differentiation) for RNA foci, DPR, and *C9orf72* mRNA levels. Mean with SD for n = 3 for each time point.

(F) Wash-out experiment. iPSC-Neurons were treated at days 3 and 8, followed by complete media change at day 13 (indicated as 10 + 0) of differentiation without compound treatment. Mean with SD for n = 3 for each time point.

Statistical analysis for (A) and (C): bar graphs depict mean with SEM, ordinary one-way ANOVA with Sidak's multiple comparison post-test, ****p < 0.0001, ***p < 0.001, **p < 0.01. Statistical analysis for (E) and (F): filled symbols indicate p < 0.05 for comparison with vehicle or ASOneg control. Detailed statistical analysis in Table S4.

infections. Here, we show that the FDA-approved guanosine/cytidine analogs decitabine, nelarabine, and entecavir reduce $(G_4C_2)_n$ foci and sense-strand-derived DPR expression in a *C9orf72* iPSC-Neuron model without significant toxicity. We confirmed the efficacy of decitabine in transgenic mice, which highlights the potential of this compound class for the treatment of patients with *C9orf72*.

iPSC-Neurons facilitate modifier screening for long-lived DPR proteins

Previously, mainly *in vitro* translation assays (Green et al., 2019) or conformation studies using synthetic $(G_4C_2)_n$ RNA have been used to identify small molecules that might block gain-of-function toxicity in *C9orf72* ALS/FTD. These compounds targeted G-quadruplex (Mori et al., 2021; Simone et al., 2018; Su et al.,
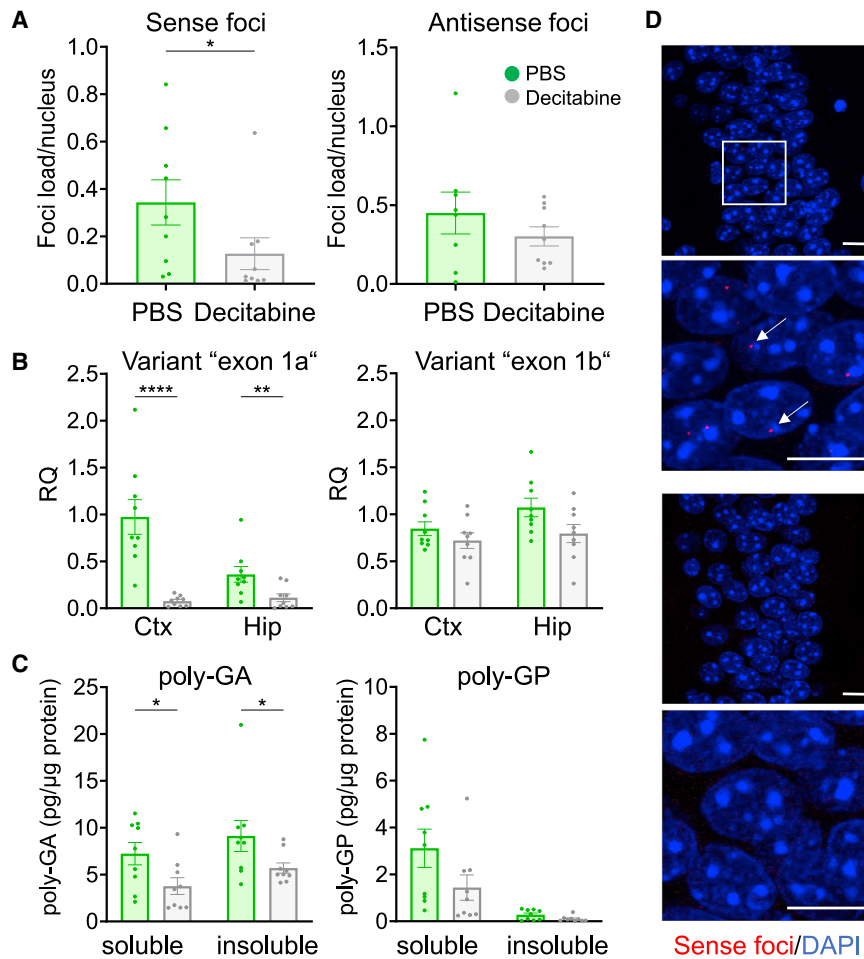
Figure 4. Decitabine reduces RNA and DPR pathology in *C9orf72* BAC mice

Nine-month-old C9[19] BAC mice (Jiang et al., 2016) treated for 7 days with decitabine at 0.6 mg/kg.

(A) Decitabine significantly reduces $(G_4C_2)_n$ sense foci in the CA1 area of hippocampus (antisense p = 0.5414) stained with FISH and quantified manually. About 6 images per mouse were examined by two independent observers and averaged.

(B) Representative images of sense RNA foci in red and nuclear staining with DAPI in blue. White arrows mark typical foci in close ups. Scale bar: 10 μm.

(C) Human *C9orf72* transgene mRNA variants were quantified by qRT-PCR in hippocampus (Hip) and cortex (Ctx).

(D) Poly-GA/GP were quantified in the neocortex from radioimmunoprecipitation assay-soluble and -insoluble fractions. Decitabine significantly affects poly-GA in both fractions. Poly-GP is mainly soluble, but reduction does not reach significance (p = 0.1135). Statistics: n = 9 transgenic mice for each treatment group. Bar graphs show mean with SEM, Mann-Whitney test: ****p < 0.0001, **p < 0.01, *p < 0.05.

Validated inhibitors

We identified and validated three inhibitors of poly-GP expression from the class of nucleoside analogs that exerted no toxicity (up to 100 μM) in iPSC-Neurons. All three compounds are clinically used, which could facilitate repurposing. Balancing CNS efficacy and systemic side effects may allow for a therapeutic window.

Nelarabine is used for chemotherapy of T cell lymphomas, blocking replication upon incorporation into genomic DNA. The active metabolites reach high micromolar concentrations (Cohen et al., 2006; Roecker et al., 2010). While chronic use in *C9orf72* ALS/FTD might not be advisable due to genotoxicity, the potential benefits of the treatment might outweigh the side effects given the low life expectancy of patients with ALS (Berg et al., 2007; Rodriguez et al., 2003).

Entecavir is a highly potent antiviral drug used to eradicate hepatitis B infections in months to years of chronic therapy (Tang et al., 2013). It acts as a specific substrate for the viral reverse transcriptase leading to strand termination but is not used by human DNA polymerases (Langley et al., 2007; Mazzucco et al., 2008), which is consistent with the minimal effects on the transcriptome in our experiments. While the dosage used for hepatitis does not reach the IC_{50} required for inhibiting DPR production in our study, primate studies already established a 100-fold safety margin for entecavir (Tang et al., 2013), suggesting the potential therapeutic safety of an effective dose.

High-dose cycles of decitabine are used to delay the clinical progression of myelodysplastic syndrome (Blum, 2010). Decitabine is incorporated into genomic DNA during replication, leading to sequestration and inactivation of DNMTs. However,

2014) and/or hairpin conformations (Wang et al., 2019) to interfere with the translation of the $(G_4C_2)_n$ repeat or selectively bind the repeat structure to assemble an endogenous nuclease and remove the transcript (Bush et al., 2021). However, synthetic RNA or reporter constructs with hundreds of $(G_4C_2)_n$ repeats could so far not be stably maintained. Very recently, others identified modifiers of DPR translation and degradation in a compound screen in HEK293 reporter cells (Licata et al., 2021). In contrast, we used iPSC-derived patient neurons that express the $(G_4C_2)_n$ repeat in its endogenous length and genomic context focusing on a repurposing approach. Our system is optimized for large-scale screening (Dhingra et al., 2020) and mimics key disease features including $(G_4C_2)_n$ foci and DPR production more closely than over-expression models or pure *in vitro* systems. Since DPRs are known to be long lived (Westergard et al., 2019), we conducted a screen with 9 days of treatment, which would be impossible in dividing cells. Since we did not notice overt toxicity in *C9orf72* iPSC-Neurons, and even treatment with targeting ASO did not result in any transcriptome-wide expression changes using our differentiation protocol, we could not test whether our hits prevent *C9orf72*-specific toxicity.

cytosine methylation was unchanged in our model, and two other DNMT inhibitors had no effects on DPR levels, implying a different mode of action for decitabine in post-mitotic neurons. Furthermore, reducing DNA methylation of the *C9orf72* gene was shown to boost its expression in dividing lymphoblasts (Liu et al., 2014). Although, we did not detect *C9orf72* upregulation in iPSC-Neurons or mouse brain, DNMT-dependent upregulation of *C9orf72* expression by decitabine in dividing myeloid cells may alleviate the loss-of-function component of *C9orf72* disease (McCauley et al., 2020; O'Rourke et al., 2016; Rizzu et al., 2016), while its effects on the $(G_4C_2)_n$ RNA may reduce gain-of-function toxicity in post-mitotic neurons. Recent approval of an oral formulation and experience with weekly low-dose off-label use in patients with sickle cell anemia not responding to conventional therapy could guide repurposing for *C9orf72* ALS/FTD (Garcia-Manero et al., 2020; Saunthararajah et al., 2008).

Mode of action

Although we initially set out to identify inhibitors of RAN translation, we found that the lead nucleoside analogs act further upstream because they still work on a $(G_4C_2)_n$ reporter containing a canonical ATG start codon and do not bind to $(G_4C_2)_{10}$ RNA. The strong effect of nucleoside analogs on sense RNA foci, the repeat-containing nascent pre-mRNA variant, its mature mRNA, and an exonic reporter constructs with only ~100 bp upstream genomic context argues for a specific effect during the elongation phase of $(G_4C_2)_n$ transcription. Similar mechanisms may apply for the $(C_4G_2)_n$ RNA based on reporter studies and the reduction of antisense foci after prolonged treatment.

Based on the similarity of the nucleoside analogs to guanosine and cytidine in the $(G_4C_2)_n$ repeat, we can only speculate about three possible mechanisms, but our data cannot distinguish between these or other possibilities: (1) low-level incorporation of the analogs into $(G_4C_2)_n$ RNA may be statistically favored by the long repeat length in most patients with *C9orf72* and may impair repeat transcription, resulting in degradation of the nascent RNA. However, widespread incorporation of the hit compounds into cellular RNA has been ruled out by us and others (Chilakala et al., 2019; Cohen et al., 2006; Oz et al., 2014). (2) Decitabine may modulate the nucleotide pool by interfering with ribonucleotide reductase or other metabolic enzymes (Gu et al., 2021), having indirect effects on $(G_4C_2)_n$ synthesis. (3) The compounds may directly inhibit DNA/RNA helicases or other proteins with nucleotide-binding sites required for transcription of the $(G_4C_2)_n$ repeat RNA in mammalian cells.

Outlook

Identifying the precise molecular target of decitabine and the other hit compounds might allow rapid screening for more potent small molecules to reduce both RNA and DPR toxicity in *C9orf72* ALS/FTD. Chemical modifications of our lead may reveal novel compounds with lower toxicity in dividing cells and further increased potency for $(G_4C_2)_n$ expression. The tolerable side effects of low-dose decitabine in chronic therapy of patients with sickle cell disease (Molokie et al., 2017), high CNS penetrance (Karahoca and Momparler, 2013), and encour-

aging results in BAC mice could justify repurposing trials in *C9orf72* patients.

Limitations of the study

Our data suggest that nucleoside analogs act on the elongation phase of transcription of the $(G_4C_2)_n$ RNA, but the precise molecular target is unknown. Antisense foci and an antisense reporter are similarly affected, but we lack sensitive assays for antisense-specific DPRs and the poorly defined endogenous antisense repeat transcript. Based on the promising wash-out experiments in cell culture, animal experiments with weekly low-dose decitabine treatment should be attempted in mice since such a schedule may be amenable to patients with *C9orf72* without risking adverse effects.

STAR★METHODS

Detailed methods are provided in the online version of this paper and include the following:

- KEY RESOURCES TABLE
- RESOURCE AVAILABILITY
  - Lead contact
  - Materials availability
  - Data and code availability
- EXPERIMENTAL MODEL AND SUBJECT DETAILS
  - iPSC-Neurons
  - Mouse model
  - Primary rat neurons
  - HEK293FT
- METHOD DETAILS
  - Compounds
  - Generation of the *C9orf72* iPSC model
  - Primary screen in iPSC derived neurons – cell culture and treatment
  - Primary rat neurons and lentivirus production
  - Decitabine treatment in *C9orf72*-BAC mice
  - Sample preparation for immunoassay
  - DPR and Tau immunoassay
  - BCA total protein assay
  - Hit selection from primary screen
  - Immunofluorescence staining
  - Fluorescence *in situ* hybridizations (FISH)
  - Quantitative RT-PCR
  - RNAseq
  - Analyzing compound binding with surface plasmon resonance (SPR)
  - Mass spectrometry (MS) analysis
  - *In vitro* transcription and translation assay
  - Cell viability assay
  - Repeat expansion fragment length analysis
  - siRNA transfection of iPSC-Neurons
- QUANTIFICATION AND STATISTICAL ANALYSIS

AUTHOR CONTRIBUTIONS

M.C. and A. Dhingra developed and executed the screen with help from C.S. and J.T. M.C. performed the immunoassays and work in heterologous cells and cloning with help from L.K. and D.F. A Dhingra performed all iPSC culture work. Q.Z. performed the mouse study with the help of E.S. E.K. helped establishing iPSC culture work in Munich. K.M. provided protocols. M.C.-L., P.R., and A. Dalmia helped with RNA-seq. D.E. analyzed the screening data. T.K. and J.M. analyzed RNA binding of compounds. T.A., F.S., M.M., and T.C. performed and analyzed MS experiments. D.E., P.H., and A Dhingra designed the study, supervised research, and acquired funding. D.E., P.H., M.C., and A Dhingra wrote the manuscript with input from all coauthors. All authors discussed the data and manuscript.

DECLARATION OF INTERESTS

T.K. and J.M. are employees of Orion Pharma. The other authors declare no competing interests.

REFERENCES

Almeida, S., Krishnan, G., Rushe, M., Gu, Y., Kankel, M.W., and Gao, F.B. (2019). Production of poly(GA) in C9ORF72 patient motor neurons derived from induced pluripotent stem cells. Acta Neuropathol. *138*, 1099–1101. https://doi.org/10.1007/s00401-019-02083-z.

Ash, P.E., Bieniek, K.F., Gendron, T.F., Caulfield, T., Lin, W.L., Dejesus-Hernandez, M., van Blitterswijk, M.M., Jansen-West, K., Paul, J.W., 3rd, Rademakers, R., et al. (2013). Unconventional translation of C9ORF72 GGGGCC expansion generates insoluble polypeptides specific to c9FTD/ALS. Neuron *77*, 639–646. https://doi.org/10.1016/j.neuron.2013.02.004.

Berg, S.L., Brueckner, C., Nuchtern, J.G., Dauser, R., McGuffey, L., and Blaney, S.M. (2007). Plasma and cerebrospinal fluid pharmacokinetics of nelarabine in nonhuman primates. Cancer Chemother. Pharmacol. *59*, 743–747. https://doi.org/10.1007/s00280-006-0328-0.

Blum, W. (2010). How much? How frequent? How long? A clinical guide to new therapies in myelodysplastic syndromes. Hematol. Am . Soc. Hematol. Educ. Program *2010*, 314–321. https://doi.org/10.1182/asheducation-2010.1.314.

Bush, J.A., Aikawa, H., Fuerst, R., Li, Y., Ursu, A., Meyer, S.M., Benhamou, R.I., Chen, J.L., Khan, T., Wagner-Griffin, S., et al. (2021). Ribonuclease recruitment using a small molecule reduced c9ALS/FTD r(G4C2) repeat expansion in vitro and in vivo ALS models. Sci. Transl. Med. *13*, eabd5991. https://doi.org/10.1126/scitranslmed.abd5991.

Busskamp, V., Lewis, N.E., Guye, P., Ng, A.H., Shipman, S.L., Byrne, S.M., Sanjana, N.E., Murn, J., Li, Y., Li, S., et al. (2014). Rapid neurogenesis through transcriptional activation in human stem cells. Mol. Syst. Biol. *10*, 760. https://doi.org/10.15252/msb.20145508.

Chew, J., Gendron, T.F., Prudencio, M., Sasaguri, H., Zhang, Y.J., Castanedes-Casey, M., Lee, C.W., Jansen-West, K., Kurti, A., Murray, M.E., et al. (2015). *C9ORF72* repeat expansions in mice cause TDP-43 pathology,

neuronal loss, and behavioral deficits. Science *348*, 1151–1154. https://doi.org/10.1126/science.aaa9344.

Chilakala, S., Feng, Y., Li, L., Mahfouz, R., Quteba, E., Saunthararajah, Y., and Xu, Y. (2019). Tracking decitabine incorporation into malignant myeloid cell DNA in vitro and in vivo by LC-MS/MS with enzymatic digestion. Sci. Rep. *9*, 4558. https://doi.org/10.1038/s41598-019-41070-y.

Cohen, M.H., Johnson, J.R., Massie, T., Sridhara, R., McGuinn, W.D., Jr., Abraham, S., Booth, B.P., Goheer, M.A., Morse, D., Chen, X.H., et al. (2006). Approval summary: nelarabine for the treatment of T-cell lymphoblastic leukemia/lymphoma. Clin. Cancer Res. *12*, 5329–5335. https://doi.org/10.1158/1078-0432.CCR-06-0606.

Cooper-Knock, J., Walsh, M.J., Higginbottom, A., Robin Highley, J., Dickman, M.J., Edbauer, D., Ince, P.G., Wharton, S.B., Wilson, S.A., Kirby, J., et al. (2014). Sequestration of multiple RNA recognition motif-containing proteins by C9orf72 repeat expansions. Brain *137*, 2040–2051. https://doi.org/10.1093/brain/awu120.

DeJesus-Hernandez, M., Mackenzie, I.R., Boeve, B.F., Boxer, A.L., Baker, M., Rutherford, N.J., Nicholson, A.M., Finch, N.A., Flynn, H., Adamson, J., et al. (2011). Expanded GGGGCC hexanucleotide repeat in noncoding region of C9ORF72 causes chromosome 9p-linked FTD and ALS. Neuron *72*, 245–256. https://doi.org/10.1016/j.neuron.2011.09.011.

Devine, M.J., Ryten, M., Vodicka, P., Thomson, A.J., Burdon, T., Houlden, H., Cavaleri, F., Nagano, M., Drummond, N.J., Taanman, J.W., et al. (2011). Parkinson's disease induced pluripotent stem cells with triplication of the alpha-synuclein locus. Nat. Commun. *2*, 440. https://doi.org/10.1038/ncomms1453.

Dhingra, A., Tager, J., Bressan, E., Rodriguez-Nieto, S., Bedi, M.S., Broer, S., Sadikoglou, E., Fernandes, N., Castillo-Lizardo, M., Rizzu, P., and Heutink, P. (2020). Automated production of human induced pluripotent stem cell-derived cortical and dopaminergic neurons with integrated live-cell monitoring. J. Vis. Exp. https://doi.org/10.3791/61525.

Donnelly, C.J., Zhang, P.W., Pham, J.T., Haeusler, A.R., Mistry, N.A., Vidensky, S., Daley, E.L., Poth, E.M., Hoover, B., Fines, D.M., et al. (2013). RNA toxicity from the ALS/FTD C9ORF72 expansion is mitigated by antisense intervention. Neuron *80*, 415–428. https://doi.org/10.1016/j.neuron.2013.10.015.

Garcia-Manero, G., Griffiths, E.A., Steensma, D.P., Roboz, G.J., Wells, R., McCloskey, J., Odenike, O., DeZern, A.E., Yee, K., Busque, L., et al. (2020). Oral cedazuridine/decitabine for MDS and CMML: a phase 2 pharmacokinetic/pharmacodynamic randomized crossover study. Blood *136*, 674–683. https://doi.org/10.1182/blood.2019004143.

Gendron, T.F., Bieniek, K.F., Zhang, Y.J., Jansen-West, K., Ash, P.E.A., Caulfield, T., Daughrity, L., Dunmore, J.H., Castanedes-Casey, M., Chew, J., et al. (2013). Antisense transcripts of the expanded C9ORF72 hexanucleotide repeat form nuclear RNA foci and undergo repeat-associated non-ATG translation in c9FTD/ALS. Acta Neuropathol. *126*, 829–844. https://doi.org/10.1007/s00401-013-1192-8.

Gijselinck, I., Van Langenhove, T., van der Zee, J., Sleegers, K., Philtjens, S., Kleinberger, G., Janssens, J., Bettens, K., Van Cauwenberghe, C., Pereson, S., et al. (2012). A C9orf72 promoter repeat expansion in a Flanders-Belgian cohort with disorders of the frontotemporal lobar degeneration-amyotrophic lateral sclerosis spectrum: a gene identification study. Lancet Neurol. *11*, 54–65. https://doi.org/10.1016/S1474-4422(11)70261-7.

Green, K.M., Glineburg, M.R., Kearse, M.G., Flores, B.N., Linsalata, A.E., Fedak, S.J., Goldstrohm, A.C., Barmada, S.J., and Todd, P.K. (2017). RAN translation at C9orf72-associated repeat expansions is selectively enhanced by the integrated stress response. Nat. Commun. *8*, 2005. https://doi.org/10.1038/s41467-017-02200-0.

Green, K.M., Sheth, U.J., Flores, B.N., Wright, S.E., Sutter, A.B., Kearse, M.G., Barmada, S.J., Ivanova, M.I., and Todd, P.K. (2019). High-throughput screening yields several small-molecule inhibitors of repeat-associated non-AUG translation. J. Biol. Chem. *294*, 18624–18638. https://doi.org/10.1074/jbc.RA119.009951.

Gu, X., Tohme, R., Tomlinson, B., Sakre, N., Hasipek, M., Durkin, L., Schuerger, C., Grabowski, D., Zidan, A.M., Radivoyevitch, T., et al. (2021). Decitabine- and 5-azacytidine resistance emerges from adaptive responses

of the pyrimidine metabolism network. Leukemia 35, 1023–1036. https://doi.org/10.1038/s41375-020-1003-x.

Guo, Q., Lehmer, C., Martinez-Sanchez, A., Rudack, T., Beck, F., Hartmann, H., Perez-Berlanga, M., Frottin, F., Hipp, M.S., Hartl, F.U., et al. (2018). In situ structure of neuronal C9orf72 poly-GA aggregates reveals proteasome recruitment. Cell 172, 696–705.e12. https://doi.org/10.1016/j.cell.2017.12.030.

Jiang, J., Zhu, Q., Gendron, T.F., Saberi, S., McAlonis-Downes, M., Seelman, A., Stauffer, J.E., Jafar-Nejad, P., Drenner, K., Schulte, D., et al. (2016). Gain of toxicity from ALS/FTD-Linked repeat expansions in C9ORF72 is alleviated by antisense oligonucleotides targeting GGGGCC-containing RNAs. Neuron 90, 535–550. https://doi.org/10.1016/j.neuron.2016.04.006.

Karahoca, M., and Momparler, R.L. (2013). Pharmacokinetic and pharmacodynamic analysis of 5-aza-2'-deoxycytidine (decitabine) in the design of its dose-schedule for cancer therapy. Clin Epigenetics 5, 3. https://doi.org/10.1186/1868-7083-5-3.

Kircher, M., Witten, D.M., Jain, P., O'Roak, B.J., Cooper, G.M., and Shendure, J. (2014). A general framework for estimating the relative pathogenicity of human genetic variants. Nat. Genet. 46, 310–315. https://doi.org/10.1038/ng.2892.

Kuhn, P.H., Wang, H., Dislich, B., Colombo, A., Zeitschel, U., Ellwart, J.W., Kremmer, E., Roßner, S., and Lichtenthaler, S.F. (2010). ADAM10 is the physiologically relevant, constitutive alpha-secretase of the amyloid precursor protein in primary neurons. EMBO J. 29, 3020–3032. https://doi.org/10.1038/emboj.2010.167.

LaClair, K.D., Zhou, Q., Michaelsen, M., Wefers, B., Brill, M.S., Janjic, A., Rathkolb, B., Farny, D., Cygan, M., de Angelis, M.H., et al. (2020). Congenic expression of poly-GA but not poly-PR in mice triggers selective neuron loss and interferon responses found in C9orf72 ALS. Acta Neuropathol. 140, 121–142. https://doi.org/10.1007/s00401-020-02176-0.

Langley, D.R., Walsh, A.W., Baldick, C.J., Eggers, B.J., Rose, R.E., Levine, S.M., Kapur, A.J., Colonno, R.J., and Tenney, D.J. (2007). Inhibition of hepatitis B virus polymerase by entecavir. J. Virol. 81, 3992–4001. https://doi.org/10.1128/JVI.02395-06.

Lehmer, C., Oeckl, P., Weishaupt, J.H., Volk, A.E., Diehl-Schmid, J., Schroeter, M.L., Lauer, M., Kornhuber, J., Levin, J., Fassbender, K., et al.; German Consortium for Frontotemporal Lobar Degeneration (2017). Poly-GP in cerebrospinal fluid links C9orf72-associated dipeptide repeat expression to the asymptomatic phase of ALS/FTD. EMBO Mol. Med. 9, 859–868. https://doi.org/10.15252/emmm.201607486.

Licata, N.V., Cristofani, R., Salomonsson, S., Wilson, K.M., Kempthorne, L., Vaizoglu, D., D'Agostino, V.G., Pollini, D., Loffredo, R., Pancher, M., et al. (2021). C9orf72 ALS/FTD dipeptide repeat protein levels are reduced by small molecules that inhibit PKA or enhance protein degradation. EMBO J. 41, e105026. https://doi.org/10.15252/embj.2020105026.

Lin, A., Giuliano, C.J., Palladino, A., John, K.M., Abramowicz, C., Yuan, M.L., Sausville, E.L., Lukow, D.A., Liu, L., Chait, A.R., et al. (2019). Off-target toxicity is a common mechanism of action of cancer drugs undergoing clinical trials. Sci. Transl. Med. 11, eaaw8412. https://doi.org/10.1126/scitranslmed.aaw8412.

Liu, E.Y., Russ, J., Wu, K., Neal, D., Suh, E., McNally, A.G., Irwin, D.J., Van Deerlin, V.M., and Lee, E.B. (2014). C9orf72 hypermethylation protects against repeat expansion-associated pathology in ALS/FTD. Acta Neuropathol. 128, 525–541. https://doi.org/10.1007/s00401-014-1286-y.

Mazzucco, C.E., Hamatake, R.K., Colonno, R.J., and Tenney, D.J. (2008). Entecavir for treatment of hepatitis B virus displays no in vitro mitochondrial toxicity or DNA polymerase gamma inhibition. Antimicrob. Agents Chemother. 52, 598–605. https://doi.org/10.1128/AAC.01122-07.

McCauley, M.E., O'Rourke, J.G., Yanez, A., Markman, J.L., Ho, R., Wang, X., Chen, S., Lall, D., Jin, M., Muhammad, A.K.M.G., et al. (2020). C9orf72 in myeloid cells suppresses STING-induced inflammation. Nature 585, 96–101. https://doi.org/10.1038/s41586-020-2625-x.

McEachin, Z.T., Gendron, T.F., Raj, N., Garcia-Murias, M., Banerjee, A., Purcell, R.H., Ward, P.J., Todd, T.W., Merritt-Garza, M.E., Jansen-West, K., et al. (2020). Chimeric peptide species contribute to divergent dipeptide repeat pathology in c9ALS/FTD and SCA36. Neuron 107, 292–305.e6. https://doi.org/10.1016/j.neuron.2020.04.011.

Menden, K., Francescatto, M., Nyima, T., Blauwendraat, C., Dhingra, A., Castillo-Lizardo, M., Fernandes, N., Kaurani, L., Kronenberg-Versteeg, D., Atarsu, B., et al. (2021). Integrated multi-omics analysis reveals common and distinct dysregulated pathways for genetic subtypes of Frontotemporal Dementia. Preprint at bioRxiv. https://doi.org/10.1101/2020.12.01.405894.

Mizielinska, S., Gronke, S., Niccoli, T., Ridler, C.E., Clayton, E.L., Devoy, A., Moens, T., Norona, F.E., Woollacott, I.O.C., Pietrzyk, J., et al. (2014). C9orf72 repeat expansions cause neurodegeneration in Drosophila through arginine-rich proteins. Science 345, 1192–1194. https://doi.org/10.1126/science.1256800.

Molokie, R., Lavelle, D., Gowhari, M., Pacini, M., Krauz, L., Hassan, J., Ibanez, V., Ruiz, M.A., Ng, K.P., Woost, P., et al. (2017). Oral tetrahydrouridine and decitabine for non-cytotoxic epigenetic gene regulation in sickle cell disease: a randomized phase 1 study. PLoS Med. 14, e1002382. https://doi.org/10.1371/journal.pmed.1002382.

Mori, K., Arzberger, T., Grasser, F.A., Gijselinck, I., May, S., Rentzsch, K., Weng, S.M., Schludi, M.H., van der Zee, J., Cruts, M., et al. (2013a). Bidirectional transcripts of the expanded C9orf72 hexanucleotide repeat are translated into aggregating dipeptide repeat proteins. Acta Neuropathol. 126, 881–893. https://doi.org/10.1007/s00401-013-1189-3.

Mori, K., Gotoh, S., Yamashita, T., Uozumi, R., Kawabe, Y., Tagami, S., Kamp, F., Nuscher, B., Edbauer, D., Haass, C., et al. (2021). The porphyrin TMPyP4 inhibits elongation during the noncanonical translation of the FTLD/ALS-associated GGGGCC repeat in the C9orf72 gene. J. Biol. Chem. 297, 101120. https://doi.org/10.1016/j.jbc.2021.101120.

Mori, K., Weng, S.M., Arzberger, T., May, S., Rentzsch, K., Kremmer, E., Schmid, B., Kretzschmar, H.A., Cruts, M., Van Broeckhoven, C., et al. (2013b). The C9orf72 GGGGCC repeat is translated into aggregating dipeptide-repeat proteins in FTLD/ALS. Science 339, 1335–1338. https://doi.org/10.1126/science.1232927.

Nakamori, M., Panigrahi, G.B., Lanni, S., Gall-Duncan, T., Hayakawa, H., Tanaka, H., Luo, J., Otabe, T., Li, J., Sakata, A., et al. (2020). A slipped-CAG DNA-binding small molecule induces trinucleotide-repeat contractions in vivo. Nat. Genet. 52, 146–159. https://doi.org/10.1038/s41588-019-0575-8.

O'Rourke, J.G., Bogdanik, L., Yanez, A., Lall, D., Wolf, A.J., Muhammad, A.K.M.G., Ho, R., Carmona, S., Vit, J.P., Zarrow, J., et al. (2016). C9orf72 is required for proper macrophage and microglial function in mice. Science 351, 1324–1329. https://doi.org/10.1126/science.aaf1064.

Oz, S., Raddatz, G., Rius, M., Blagitko-Dorfs, N., Lubbert, M., Maercker, C., and Lyko, F. (2014). Quantitative determination of decitabine incorporation into DNA and its effect on mutation rates in human cancer cells. Nucleic Acids Res. 42, e152. https://doi.org/10.1093/nar/gku775.

Paila, U., Chapman, B.A., Kirchner, R., and Quinlan, A.R. (2013). GEMINI: integrative exploration of genetic variation and genome annotations. PLoS Comput. Biol. 9, e1003153. https://doi.org/10.1371/journal.pcbi.1003153.

Renton, A.E., Majounie, E., Waite, A., Simon-Sanchez, J., Rollinson, S., Gibbs, J.R., Schymick, J.C., Laaksovirta, H., van Swieten, J.C., Myllykangas, L., et al. (2011). A hexanucleotide repeat expansion in C9ORF72 is the cause of chromosome 9p21-linked ALS-FTD. Neuron 72, 257–268. https://doi.org/10.1016/j.neuron.2011.09.010.

Rizzu, P., Blauwendraat, C., Heetveld, S., Lynes, E.M., Castillo-Lizardo, M., Dhingra, A., Pyz, E., Hobert, M., Synofzik, M., Simon-Sanchez, J., et al. (2016). C9orf72 is differentially expressed in the central nervous system and myeloid cells and consistently reduced in C9orf72, MAPT and GRN mutation carriers. Acta Neuropathol. Commun. 4, 37. https://doi.org/10.1186/s40478-016-0306-7.

Rodriguez, C.M., and Todd, P.K. (2019). New pathologic mechanisms in nucleotide repeat expansion disorders. Neurobiol. Dis. 130, 104515. https://doi.org/10.1016/j.nbd.2019.104515.

Rodriguez, C.O., Jr., Stellrecht, C.M., and Gandhi, V. (2003). Mechanisms for T-cell selective cytotoxicity of arabinosylguanine. Blood *102*, 1842–1848. https://doi.org/10.1182/blood-2003-01-0317.

Roecker, A.M., Stockert, A., and Kisor, D.F. (2010). Nelarabine in the treatment of refractory T-cell malignancies. Clin. Med. Insights Oncol. *4*, CMO.S4364. https://doi.org/10.4137/CMO.S4364.

Saunthararajah, Y., Molokie, R., Saraf, S., Sidhwani, S., Gowhari, M., Vara, S., Lavelle, D., and DeSimone, J. (2008). Clinical effectiveness of decitabine in severe sickle cell disease. Br. J. Haematol. *141*, 126–129. https://doi.org/10.1111/j.1365-2141.2008.07027.x.

Simone, R., Balendra, R., Moens, T.G., Preza, E., Wilson, K.M., Heslegrave, A., Woodling, N.S., Niccoli, T., Gilbert-Jaramillo, J., Abdelkarim, S., et al. (2018). G-quadruplex-binding small molecules ameliorate C9orf72 FTD/ALS pathology in vitro and in vivo. EMBO Mol. Med. *10*, 22–31. https://doi.org/10.15252/emmm.201707850.

Su, Z., Zhang, Y., Gendron, T.F., Bauer, P.O., Chew, J., Yang, W.Y., Fostvedt, E., Jansen-West, K., Belzil, V.V., Desaro, P., et al. (2014). Discovery of a biomarker and lead small molecules to target r(GGGGCC)-associated defects in c9FTD/ALS. Neuron *83*, 1043–1050. https://doi.org/10.1016/j.neuron.2014.07.041.

Swinnen, B., Robberecht, W., and Van Den Bosch, L. (2020). RNA toxicity in non-coding repeat expansion disorders. EMBO J. *39*, e101112. https://doi.org/10.15252/embj.2018101112.

Tabet, R., Schaeffer, L., Freyermuth, F., Jambeau, M., Workman, M., Lee, C.Z., Lin, C.C., Jiang, J., Jansen-West, K., Abou-Hamdan, H., et al. (2018). CUG initiation and frameshifting enable production of dipeptide repeat proteins from ALS/FTD C9ORF72 transcripts. Nat. Commun. *9*, 152. https://doi.org/10.1038/s41467-017-02643-5.

Taghizadeh, K., McFaline, J.L., Pang, B., Sullivan, M., Dong, M., Plummer, E., and Dedon, P.C. (2008). Quantification of DNA damage products resulting from deamination, oxidation and reaction with products of lipid peroxidation by liquid chromatography isotope dilution tandem mass spectrometry. Nat. Protoc. *3*, 1287–1298. https://doi.org/10.1038/nprot.2008.119.

Takahashi, K., Tanabe, K., Ohnuki, M., Narita, M., Ichisaka, T., Tomoda, K., and Yamanaka, S. (2007). Induction of pluripotent stem cells from adult human fibroblasts by defined factors. Cell *131*, 861–872. https://doi.org/10.1016/j.cell.2007.11.019.

Tang, H., Griffin, J., Innaimo, S., Lehman-Mckeeman, L., and Llamoso, C. (2013). The Discovery and development of a potent antiviral drug, entecavir, for the treatment of chronic hepatitis B. J. Clin. Transl. Hepatol. *1*, 51–58. https://doi.org/10.14218/JCTH.2013.00006.

Traube, F.R., Schiffers, S., Iwan, K., Kellner, S., Spada, F., Muller, M., and Carell, T. (2019). Isotope-dilution mass spectrometry for exact quantification of noncanonical DNA nucleosides. Nat. Protoc. *14*, 283–312. https://doi.org/10.1038/s41596-018-0094-6.

Truett, G.E., Heeger, P., Mynatt, R.L., Truett, A.A., Walker, J.A., and Warman, M.L. (2000). Preparation of PCR-quality mouse genomic DNA with hot sodium hydroxide and tris (HotSHOT). Biotechniques *29*, 52–54. https://doi.org/10.2144/00291bm09.

Vesely, J., and Cihak, A. (1977). Incorporation of a potent antileukemic agent, 5-aza-2'-deoxycytidine, into DNA of cells from leukemic mice. Cancer Res. *37*, 3684–3689.

Waite, A.J., Baumer, D., East, S., Neal, J., Morris, H.R., Ansorge, O., and Blake, D.J. (2014). Reduced C9orf72 protein levels in frontal cortex of amyotrophic lateral sclerosis and frontotemporal degeneration brain with the C9ORF72 hexanucleotide repeat expansion. Neurobiol. Aging *35*, 1779.e5. https://doi.org/10.1016/j.neurobiolaging.2014.01.016.

Wang, Z.F., Ursu, A., Childs-Disney, J.L., Guertler, R., Yang, W.Y., Bernat, V., Rzuczek, S.G., Fuerst, R., Zhang, Y.J., Gendron, T.F., et al. (2019). The hairpin form of r(G4C2)(exp) in c9ALS/FTD is repeat-associated non-ATG translated and a target for bioactive small molecules. Cell Chem. Biol. *26*, 179–190.e12. https://doi.org/10.1016/j.chembiol.2018.10.018.

Westergard, T., McAvoy, K., Russell, K., Wen, X., Pang, Y., Morris, B., Pasinelli, P., Trotti, D., and Haeusler, A. (2019). Repeat-associated non-AUG translation in C9orf72-ALS/FTD is driven by neuronal excitation and stress. EMBO Mol. Med. *11*, e9423. https://doi.org/10.15252/emmm.201809423.

Yu, G., Wang, L.G., Han, Y., and He, Q.Y. (2012). clusterProfiler: an R package for comparing biological themes among gene clusters. OMICS *16*, 284–287. https://doi.org/10.1089/omi.2011.0118.

Zhang, Y., Pak, C., Han, Y., Ahlenius, H., Zhang, Z., Chanda, S., Marro, S., Patzke, C., Acuna, C., Covy, J., et al. (2013). Rapid single-step induction of functional neurons from human pluripotent stem cells. Neuron *78*, 785–798. https://doi.org/10.1016/j.neuron.2013.05.029.

Zhou, Q., Lehmer, C., Michaelsen, M., Mori, K., Alterauge, D., Baumjohann, D., Schludi, M.H., Greiling, J., Farny, D., Flatley, A., et al. (2017). Antibodies inhibit transmission and aggregation of C9orf72 poly-GA dipeptide repeat proteins. EMBO Mol. Med. *9*, 687–702. https://doi.org/10.15252/emmm.201607054.

Zhou, Q., Mareljic, N., Michaelsen, M., Parhizkar, S., Heindl, S., Nuscher, B., Farny, D., Czuppa, M., Schludi, C., Graf, A., et al. (2020). Active poly-GA vaccination prevents microglia activation and motor deficits in a C9orf72 mouse model. EMBO Mol. Med. *12*, e10919. https://doi.org/10.15252/emmm.201910919.

Zu, T., Gibbens, B., Doty, N.S., Gomes-Pereira, M., Huguet, A., Stone, M.D., Margolis, J., Peterson, M., Markowski, T.W., Ingram, M.A.C., et al. (2011). Non-ATG-initiated translation directed by microsatellite expansions. Proc. Natl. Acad. Sci. U. S. A. *108*, 260–265. https://doi.org/10.1073/pnas.1013343108.

Zu, T., Guo, S., Bardhi, O., Ryskamp, D.A., Li, J., Khoramian Tusi, S., Engelbrecht, A., Klippel, K., Chakrabarty, P., Nguyen, L., et al. (2020). Metformin inhibits RAN translation through PKR pathway and mitigates disease in C9orf72 ALS/FTD mice. Proc. Natl. Acad. Sci. U. S. A. *117*, 18591–18599. https://doi.org/10.1073/pnas.2005748117.

Zu, T., Liu, Y., Banez-Coronel, M., Reid, T., Pletnikova, O., Lewis, J., Miller, T.M., Harms, M.B., Falchook, A.E., Subramony, S.H., et al. (2013). RAN proteins and RNA foci from antisense transcripts in C9ORF72 ALS and frontotemporal dementia. Proc. Natl. Acad. Sci. U. S. A. *110*, E4968–E4977. https://doi.org/10.1073/pnas.1315438110.

STAR★METHODS

KEY RESOURCES TABLE

REAGENT or RESOURCE	SOURCE	IDENTIFIER
Antibodies		
rat monoclonal anti-GP (18H8)	Antibody Facility, Helmholtz Zentrum München (Lehmer et al., 2017)	N/A
rat monoclonal anti-GP (3F9)	Antibody Facility, Helmholtz Zentrum München (Lehmer et al., 2017)	N/A
Mouse monoclonal anti-GA (1A12)	Antibody Facility, Helmholtz Zentrum München (Zhou et al., 2020)	N/A
Tuj-1	R and D Systems	Cat# MAB1195; RRID: AB_357520
BRN-2	Cell Signaling	Cat# 12137; RRID: AB_2797827
yH2A.X	Merck Millipore	Cat# 05-636; RRID: AB_309864
Map2	Merck Millipore	Cat# AB5622; RRID: AB_91939
Chemicals, peptides, and recombinant proteins		
16% Formaldehyde-100 mL	Sigma	C6645-100MG
5-Aza-2'-deoxycytidine-5'-triphosphate, Sodium salt	Jena Bioscience	NU-1118
5'-Fluoro-2'-deoxycytidine	Merck Millipore	F5307
Accutase	Life Technologies	A11105-01
Actinomycin D	Sigma	A9415
B27 supplement	Life Technologies	17504044
BDNF	Peprotech	450-03
DAPT	Merck Millipore	420220-10MG
Decitabine	Selleck	S1200
Dextran sulphate	Merck Millipore	3730-100ML
DMEM, high glucose, GlutaMAX	Thermo Fisher	10566-016
Entecavir Hydrate	Selleck	S1252
FDA-approved Drug Library	Selleck	L1300
Fetal calf serum (FCS)	Sigma	F7524
Formamide	MP biomedical	11FORMD002
GDNF	Peprotech	450-02
Gel Loading Buffer II	Invitrogen	AM8546G
HEPES	Thermo Fisher	15630080
Laminin	Sigma	L2020-1MG
L-glutamine	Gibco	25030081
Matrigel	Corning	354277
MEM non-essential amino acids solution (NEAA)	Thermo Fisher	11140050
NEAA	Life Technologies	11140-035
Nelarabine	Selleck	S1213
Neurobasal Medium	Life Technologies	21103049
NT-3	Peprotech	450-10
Penicillin-Streptomycin (10,000 U/mL)	Life Technologies	15140-122
poly L-ornithine	Sigma	P3655
protease inhibitor cocktail	Sigma	P8340-5ML
Ralimetinib	Selleck	S1494
RG108	Selleck	S2821
Ribonucleoside Vanadyl Complex	NEB	S1402S - 200 mM

(Continued on next page)

Continued

REAGENT or RESOURCE	SOURCE	IDENTIFIER
Ribonucleoside Vanadyl Complex	NEB	S1402S - 200 mM
RQ1 RNase-Free DNase	Promega	M6101
Saline Sodium Citrate (SSC) buffer	Sigma Aldrich	S6639-1L
Sodium phosphate buffer pH 7	Sigma Aldrich	SRE0064-500M
Tanespimycin (17-AAG)	Selleck	S1141
Critical commercial assays		
MSD total Tau kit	Mesoscale	K151DSD
MSD GOLD SULFO-TAG™ NHS-Ester	Mesoscale	R91AO-1
MSD Gold 96-well Streptavidin SECTOR plates	Mesoscale	L15SA
Pierce™ BCA Protein Assay Reagent	Thermo Fisher	#23222+23224
RNeasy Mini Kit	Qiagen	74104
RNeasy Plus Mini Kit	Qiagen	74134
RNeasy Micro Kit	Qiagen	74004
Direct-zol-96 RNA kit	Zymo Research	R2054
Zymo-Spin IIC columns	Zymo Research	C1011
High-Capacity RNA-to-cDNA™ Kit	Applied Biosystems	4387406
M-MLV Reverse Transcriptase	Promega	M1701
TaqMan™ microRNA Kit	Life Technologies	4366596
SYBR™ Select Mastermix	Thermo Fisher	4472903
Illumina Stranded mRNA Prep, Ligation	Illumina	20040532
IDT for Illumina RNA UD Indexes Set B	Illumina	20040554
AmplideX PCR/CE C9orf72 Kit	Asuragen	49581
NextSeq 500/550 High Output Kit v2.5	Illumina	20024906
Nucleoside Digestion Mix	NEB	M0649S
RiboMAX Large Scale RNA Production System T7	Promega	P1300
Flexi Rabbit Reticulocyte Lysate System	Promega	L4540
NucleoSpin Gel and PCR Clean-up Kit	Macherey-Nagel	740609.250
RNA Clean & Concentrator-25 kit	Zymo	R1017
Century-Plus RNA Marker	Ambion	AM7145
LIVE/DEAD™ Viability/Cytotoxicity Kit, for mammalian cells	Thermo Fisher	L3224
peqGOLD, DNasI Digest kit	Peglab, VWR	13-1091-00
SuperScript™ VILO™ cDNA Synthesis	Thermo Fisher	11754050
Lipofectamine RNAiMAX Transfection Reagent	Thermo Fisher	13778150
Lipofectamine 2000 Transfection Reagent	Thermo Fisher	11668019
VECTASHIELD Vibrance Antifade Mounting Medium with DAPI	Vector Labs	H-1200-10
Click-it Nascent RNA Capture Kit	Life Technologies	C10365
TRIzol™ Reagent	Thermo Fisher	15596026
SuperScript™ VILO™ cDNA Synthesis Kit	Thermo Fisher	11754050
PrimeTime Gene Expression Master Mix	IDT	1055772
mouse housekeeping probe assay: B2m	IDT	Mm.PT.39a.22214835
mouse housekeeping probe assay: Actb	IDT	Mm.PT.39a.22214843.g
rat housekeeping probe assay: GAPDH	IDT	Rn.PT.39a.11180736.g
human housekeeping probe assay: GAPDH	IDT	Hs.PT.39a.22214836
human C9orf72 probe assay (exon 1a)	IDT	Hs.PT.58.1275101
human C9orf72 probe assay (exon 1b)	IDT	Hs.PT.58.4064580
human C9orf72 probe assay (exon 3-5)	IDT	Hs.PT.58.38350554

Continued

REAGENT or RESOURCE	SOURCE	IDENTIFIER
Human MLH1 probe assay	IDT	Hs.PT.58.40186049.g
Human MLH2 probe assay	IDT	Hs.PT.58.25954157
Human MLH3 probe assay	IDT	Hs.PT.58.15434768
Human MLH4 probe assay	IDT	Hs.PT.58.39275522
Human MSH2 probe assay	IDT	Hs.PT.58.38933026.g
Human XRCC6 probe assay	IDT	Hs.PT.58.21136061
Human FEN1 probe assay	IDT	Hs.PT.58.1554556
Human XPA probe assay	IDT	Hs.PT.58.1683980
Human XPB probe assay	IDT	Hs.PT.58.15606497
Human XPC probe assay	IDT	Hs.PT.58.26563606
Silencer Select siRNA C9orf72	Invitrogen	s530921, s530920
Silencer Select siRNA MLH1	Invitrogen	s297, s224048, s298
Silencer Select siRNA MLH2	Invitrogen	s10728, s229952, s229951
Silencer Select siRNA MLH3	Invitrogen	s534082, s25712, s534081
Silencer Select siRNA MLH4	Invitrogen	s10740, s10742, s534926
Silencer Select siRNA MSH2	Invitrogen	s534362, s8966, s8967
Silencer Select siRNA XRCC6	Invitrogen	s5457, s5456, s52594
Silencer Select siRNA FEN1	Invitrogen	s5104, s5105, s5103
Silencer Select siRNA XPA	Invitrogen	s14926, s14927, s14925
Silencer Select siRNA XPB	Invitrogen	s4796, s533737, s4797
Silencer Select siRNA XPC	Invitrogen	s14929, s533961, s14928
Silencer Select siRNA negative control	Invitrogen	s813
Deposited data		
RNAseq data	EGA	EGAS00001006138
Experimental models: cell lines		
C9 iPSC line	NINDS collection	NN0004306
C9 iPSC line	NINDS collection	NN0000035
C9 iPSC line	NINDS collection	NN0004307
Fibroblasts for reprogramming	J. Hardy, S. Wray, University College London	STCL49
Control iPSC line	Coriell Institute, https://www.coriell.org	GM23280
Control iPSC line	T. Kunath, University of Edinburgh (Devine et al., 2011)	NAS7
Control iPSC line	NINDS collection	ND41865
HEK293FT cell line	Thermo Fisher	R70007
Experimental models: organisms/strains		
C9[19] BAC transgenic mouse line B6N.Cg-Tg(C9orf72*)19Lagi/J	Jiang et al., 2016	MGI:J:232242
CD Sprague-Dawley IGS rats	Charles River	CD-SIFA; RRID: RGD_734476
Oligonucleotides		
ASOpos TGGTTAATmCTTTATmCAGGTmC	Jiang et al., 2016	N/A
ASOneg mCmCTATAGGAmCTATmCmCAGGAA	Microsynth AG	N/A
Antisense LNA probes (CCCCGG)$_{2.5}$ (Lot: 274175518)	Jiang et al., 2016	339501
Sense LNA probes (GGGGCC)$_{2.5}$ (Lot: 274175516)	Microsynth AG	339501
qPCR and genotyping primer information: Table S5	N/A	N/A

(Continued on next page)

Continued

REAGENT or RESOURCE	SOURCE	IDENTIFIER
Recombinant DNA		
pSPAX	Gift from Didier Trono	RRID: Addgene_12260
pcDNA3.1-VSVG	Kuhn et al., 2010	N/A
FhSynW2 TA$(G_4C_2)_{100}$	This study	N/A
FhSynW2 AT$(G_4C_2)_{50}$	This study	N/A
FhSynW2 $(C_4G_2)_{50}$	This study	N/A
pEF6 $(G_4C_2)_{60}$	Zhou et al., 2017	N/A
pLV_TRET_hNgn2_UBC_BSD_T2A_rtTA3	Menden et al., 2021	N/A
Software and algorithms		
GraphPad Prism 8.4.3	GraphPad Software	www.graphpad.com/scientific-software/prism/
ImageJ (v1.53o)	N/A	https://imagej.nih.gov/ij/
Zen (blue edition)	Carl Zeiss Microscopy GmbH	https://www.zeiss.de/mikroskopie/produkte/mikroskopsoftware/zen-lite.html
Graphical Schemes	BioRender.com	https://biorender.com/
Bio-Rad CFX Manager 3.1	BioRad	#1845000
CLC genomics workbench 21.0.3	Qiagen	https://digitalinsights.qiagen.com/
Cell pathfinder	Yokogawa Electric Corporation	https://www.yokogawa.com/eu/solutions/products-platforms/life-science/high-content-analysis/analysis-software/cellpathfinder/
MassHunter Workstation Software Quantitative Analysis Version B.07.01 / Build 7.1.524.0 for QQQ	Agilent	N/A
Columbus	Perkin Elmer	https://www.perkinelmer.com/product/image-data-storage-and-analysis-system-columbus
Genemarker 3.1	Soft Genetics	https://softgenetics.com/specs.php
clusterProfiler 4.2.2	Yu et al., 2012	https://bioconductor.org/packages/release/bioc/html/clusterProfiler.html

RESOURCE AVAILABILITY

Lead contact
Further information and requests for resources and reagents should be directed to and will be fulfilled by the lead contact, Dieter Edbauer (dieter.edbauer@dzne.de).

Materials availability
This study did not generate new unique reagents, plasmids or animal lines.

Data and code availability
- Raw data from RNAseq experiments have been deposited at the European Genome-phenome Archive (EGA), which is hosted by the EBI and the CRG, under accession number EGA: EGAS00001006138. Fully analyzed data is included in the supplemental tables.
- This paper does not report original code.
- Any additional information required to reanalyze the data reported in this paper is available from the lead contact upon request.

EXPERIMENTAL MODEL AND SUBJECT DETAILS

iPSC-Neurons
Fibroblasts of an individual with *C9orf72* expansion (provided by John Hardy and Selina Wray, University College London) were reprogrammed into iPSCs as described in the below method details section. Four *C9orf72* iPSC lines NN0004306, NN0004307, NN0004309 and NN0000035 obtained from NINDS collection from Rutgers, (https://bioq.nindsgenetics.org/) and three control lines

ND41865 (from NINDS), NAS7 (obtained from Dr. Tilo Kunath, University of Edinburgh), GM23280 (from Coriell Insitute, https://www.coriell.org/).

Mouse model

The C9[19] BAC transgenic mouse line (B6N.Cg-Tg(C9orf72*)19Lagi/J) generated by (Jiang et al., 2016) was imported from the Jackson laboratory and maintained in C57BL/6N background and treated at 9 months of age (see below). Littermates of the same sex were randomly assigned to experimental groups. Animal experiments were performed in accordance with institutional guidelines approved by the government of Upper Bavaria (protocol Vet_02-17-106) and housed in standard cages in a pathogen-free facility on a 12 h light/dark cycle with ad libitum access to food and water.

Primary rat neurons

Primary rat neurons were isolated from embryonic day 19 CD Sprague-Dawley IGS rats (CD-SIFA; RRID: RGD 734476) imported from Charles River and housed in a pathogen-free facility with 12 h light/dark cycle and food/water available ad libitum in compliance with institutional policies approved by the government of Upper Bavaria following §11 Abs.1 TierSchG for the DZNE animal facility (Inst.-Nr. 04-26). The neurons were plated and cultivated in Neurobasal Medium (Life Technologies) supplemented with 2% B27 (Life Technologies), 1% Penicillin-Streptomycin and 0.5 mM L-glutamine (Gibco) at 37°C in 5% CO_2 in 12-well plates.

HEK293FT

HEK293FT cells (female) used for siRNA validation experiments were obtained from Thermo Fisher Scientific #R70007. Cells were cultured in DMEM Glutamax medium (Thermo Fisher) supplemented with 10% Fetal calf serum (FCS) (Sigma), 1% Penicillin-Streptomycin (Life Technologies) and 1% non-essential amino acids (NEAA) (Thermo) at 37°C and 5% CO2.

METHOD DETAILS

Compounds

An FDA-approved drug library for the poly-GP screen was purchased at Selleck chem (# L1300) and contained 1430 compounds in a 96-well format. For validation, compounds were reordered individually: Entecavir Hydrate (Selleck, S1252), Nelarabine (Selleck, S1213), Decitabine (Selleck, S1200), Ralimetinib (Selleck, S1494), Tanespimycin (17-AAG) (Selleck, S1141), RG108 (Selleck, S2821), 5-Fluoro-2'-deoxycytidine (Merck, F5307). All compounds were dissolved in DMSO to a final concentration of 20 mM. Screening and all assays in 96-well format were done at 1% DMSO, validation in 12- and 6-well format was done at 0.1% DMSO.

Validated antisense oligonucleotides (ASO) targeting *C9orf72* intron 1 (TGGTTAATmCTTTATmCAGGTmC) and a control ASO (mCmCTATAGGAmCTATmCmCAGGAA) were synthesized as 5-10-5 MOE gapmers as previously described (Microsynth AG, Switzerland) (Jiang et al., 2016). Each internucleoside linkage was a phosphorothioate linkage, and each of the nucleosides 1-5 and 16-20 comprised a 2'-O-methoxyethyl modified ribonucleotide with ten 2'-deoxynucleosides in-between.

Generation of the *C9orf72* iPSC model

Fibroblasts of an individual with *C9orf72* expansion (provided by John Hardy and Selina Wray, University College London) were reprogrammed into iPSCs using pVSV-G pseudotyped retroviral transduction of the Yamanaka factors (OSKM) (Takahashi et al., 2007). iPSCs were cultured in Essential-8 flex medium (Thermo Fisher) on Matrigel in feeder-free conditions. iPSCs were characterized for the expression of typical stem cell markers and *in vitro* differentiation to three germ layers (not shown) and routinely checked for the absence of mycoplasma contamination. To check for genome integrity, two sub-clones were whole-genome sequenced using Illumina NovaSeq6000. These raw data were variant called using the standard GATK4 best-practices pipeline for single-nucleotide polymorphism and indel discovery. The normalized and annotated VCF was queried for rare variants with minor allele frequency (less than 0.01) and CADD score > 20 using GEMINI software (Kircher et al., 2014; Paila et al., 2013). We concluded that none of the sub-clones carries rare disease-causing variants for any neurodegenerative diseases or related traits. Four additional *C9orf72* iPSC lines (NN0004306 with ~70 repeats, NN0004307 and NN0004309 with ~800 repeats each and NN0000035 with >145 repeats) and three control lines, ND41865 (obtained from NINDS collection from Rutgers (https://bioq.nindsgenetics.org/)), GM23280 (iPSC line was obtained from the Coriell Institute (https://www.coriell.org/)) and NAS7 (cell line has been obtained from Dr. Tilo Kunath (University of Edinburgh), described in (Devine et al., 2011). Hexanucleotide repeat expansion in *C9orf72* was confirmed using repeat-primed PCR (AmplideX PCR/CE *C9orf72* Kit, Asuragen).

Primary screen in iPSC derived neurons – cell culture and treatment

The differentiation protocol was performed as described (Dhingra et al., 2020). In short, smNPC stable inducible line for NGN2 expression was generated using a single lentivirus vector system consisting of pLV_TRET_hNgn2_UBC_BSD_T2A_rtTA3 (Menden et al., 2021). Stable NGN2 smNPCs were used within 8 passages post-transduction.

For screening, the cells were plated (50,000 cells/well) onto 0.01% poly L-ornithine coated plates (96-well cell carrier, Perkin Elmer) in the N2B27 medium (Dhingra et al., 2020) supplemented with 2.5 μg/mL doxycycline at, 2 μM DAPT and 5 μg/mL laminin (on-the-go coating) using Multiflo Fx dispenser (Biotek). On day 3 of differentiation, compounds were added (final 10 μM in 1% DMSO) using an

automated cell culture system (Dhingra et al., 2020) in six replicate plates, using N2B27 media supplemented with 2.5 μg/mL doxy-cycline, 10 ng/mL brain-derived neurotrophic factor (BDNF), 10 ng/mL glial cell-derived neurotrophic factor (GDNF), 10 ng/mL neuro-trophic factor 3 (NT-3), 1 μg/mL laminin, and 10 μM DAPT. The compound treatment was repeated on day 8 of differentiation without adding additional doxycycline or DAPT. ASOs were added on day 3 and 8 at 2 μM final concentration. On day 12 of differentiation (i.e. day 9 of compound treatment) the media was aspirated using Integra VIAFLO (96-well head), cells were gently washed with 150 μL PBS and stored at −80°C until processed for MesoScale Discovery (MSD) assay. For larger volume format, plates were coated with poly L-ornithine (0.01%) and laminin (5 μg/mL) for 4 hours before plating cells.

To minimize edge-effects we used only the inner 60 wells of each plate and randomly distributed 50 compounds (10 μM in 1% DMSO or PBS), 4 solvent controls for within-plate normalization (1% DMSO or PBS), 3 ASO negative controls and 3 ASO positive controls. In total 30 different compound plates were measured in 6 replicates each, while the multiple controls per plate were analyzed individually.

Primary rat neurons and lentivirus production

Neuron cultures were prepared from embryonic day 19 CD Sprague-Dawley IGS rats of both sexes. Neocortex and hippocampus were dissected in ice-cold dissection media (HBBS with 1% Penicillin-Streptomycin and additional 10 mM HEPES pH 7.3). The tissue was enzymatically dissociated at 37°C (for cortices 20 min in 0.25% trypsin, 0.7 mg/mL DNase I; for hippocampi 15 min in 0.15% trypsin in dissection media) followed by gentle trituration. For biochemical experiments, 400,000 cells/mL cortical neurons were plated on 12-well plates coated with poly-D-lysine and cultured in Neurobasal medium containing 2% B27 (Thermo Fisher), penicillin-strep-tomycin, 0.5 mM L-glutamine (Thermo Fisher) and incubated at 37°C in 5% CO_2. For immunofluorescence experiments, 85,000 cells/mL hippocampal neurons we plated on coverslips in 12-well plates and cultured as above with additional 12.5 μM L-glutamate.

Primary neurons were transduced with lentiviral constructs FhSynW TA($G_4C_2)_{100}$, FhSynW AT($G_4C_2)_{50}$ and FhSynW ($C_4G_2)_{50}$, which was cloned by reversing the insert from TA($G_4C_2)_{100}$ and thus lacks the endogenous upstream region. Lentiviral particles were produced as described previously (Guo et al., 2018). Briefly, HEK293FT cells were seeded in 10 cm dishes ($5*10^6$ cells/10 cm dish) and the next day transfected with lentivirus packaging vectors (pSPAX, pVSV-G) and the construct of interest using Lip-ofectamine 2000 (Invitrogen). After 24 hours the media was changed to packaging media with 13 mg/mL bovine serum albumin (BSA) and after another 24 hours the supernatant was harvested, the viral particles were concentrated by ultracentrifugation, then resus-pended in neurobasal medium and stored at −80°C.

Neurons were transduced at DIV6 and compound treatment at 10 μM (ASO treatment at 2 μM) concentration was performed on DIV7. At DIV10 neurons were rinsed with PBS and stored at −80°C for later lysis with RIPA buffer for immunoassay measurements or RNA extraction for qPCR analysis.

Decitabine treatment in *C9orf72*-BAC mice

The C9[19] BAC transgenic mouse line (B6N.Cg-Tg(C9orf72*)19Lagi/J) generated by (Jiang et al., 2016) was imported from the Jack-son laboratory and maintained in C57BL/6N background. For genotyping, mouse genomic DNA was prepared using Hot Sodium Hy-droxide and Tris (HotSHOT) method as described previously (Truett et al., 2000). Genotyping PCR was performed using primers (CATCCCAGACAAGAAATCATGG and CCGTCGACATTTAGGTGACA) for the transgene. The presence of the full-length transgene was confirmed with Southern blot as described previously (Jiang et al., 2016).

For compound treatment, 9-month-old transgenic animals received daily 0.6 mg/kg decitabine by i.p. injection for 7 consecutive days (Vesely and Cihak, 1977). Littermates of the same sex were randomly assigned to experimental groups. Animal handling and animal experiments were performed in accordance with institutional guidelines approved by local animal laws and housed in stan-dard cages in a pathogen-free facility on a 12 h light/dark cycle with ad libitum access to food and water.

Sample preparation for immunoassay

For lysis, the frozen sample plates were thawed on ice for 10 min before adding RIPA buffer (137 mM NaCl, 20 mM Tris pH7.5, 10% glycerol, 1% Triton X-100, 0.5% sodium deoxycholate, 0.1% SDS, 2 mM EDTA) supplemented with protease inhibitor cocktail (Sigma, #P8340). 96-well format samples were lysed in 80 μL buffer, 12-well format samples were lysed in 400 μL and 6-well format samples in 800 μL buffer per well. After 30 min incubation on ice, the samples were mixed using a 96-well semi-automated pipette (Integra Viaflo) and stored at −80°C until measurement.

To generate RIPA soluble and insoluble fractions from mice, mouse brain samples were homogenized in 600 μL RIPA buffer (sup-plemented with protease and phosphatase inhibitors, and benzonase nuclease) using a tissue homogenizer (Precellys). Samples were incubated while shaking at 4°C for 20 min and centrifuged at 13,000 g for 10 min at 4°C. To avoid cross-contamination between soluble and insoluble fractions, pellets were resuspended in 1 mL RIPA, re-homogenized, and re-centrifuged. The RIPA-insoluble pellets were homogenized in 300 μL RIPA buffer containing 3.5 M Urea (U-RIPA), and protein concentration was determined by BCA assay.

DPR and Tau immunoassay

The immunoassays were performed on the MSD platform using streptavidin plates (MSD Gold 96-well Streptavidin SECTOR: #L15SA). The plates were coated over-night at 4°C with 100 μL/well biotinylated capture antibody in blocking buffer (PBS with

0.05% Tween-20, 1% BSA). After washing (PBS with 0.05% Tween-20) using a BioTek 405LS Microplate washer, the plates were incubated with 60 μL/well of cell lysate samples (lysate preparation above) for 2 h at room temperature on a shaking platform (140 rpm). After three washing steps, 100 μL/well sulfo-tag-labeled detection antibody diluted in blocking buffer was added and the plates were incubated for 2 h as described above, followed by three final washing steps. After adding 100 μL MSD Read Buffer T, the electrochemiluminescent signal was measured using a MESO QuickPlex SG120 instrument. Antibodies used for poly-GP measurement were biotinylated 18H8 (0.13 μg/mL) and sulfo-tagged 3F9 (1 μg/mL). To measure poly-GA levels we used biotinylated 1A12 (1 μg/mL) and sulfo-tagged 1A12 (1 μg/mL) antibodies. The measurement of total-Tau was performed following the guidelines of the MSD total Tau kit (Mesoscale: #K151DSD) after diluting the lysates 1:20 with RIPA buffer.

BCA total protein assay

Total protein levels in all lysates were quantified using Pierce™ BCA Protein Assay Reagents (Thermo Fisher: #23222 and #23224). After the incubation step for the poly-GP immunoassay, 30 μL of the lysed sample was transferred from the MSD plates to fresh 96-well plates and 200 μL of the BCA reagent mix was added to each well. After 1 h incubation at room temperature, plates were measured using a BioTek Cytation 3 Multi-Mode Reader at 562 nm. A BSA dilution series on every plate was used as standard curve. For the primary screen, all samples were normalized to the mean BCA values of the solvent controls instead.

Hit selection from primary screen

The raw poly-GP and BCA levels were normalized to the 4 solvent controls within each plate after subtracting the blank value. Relative poly-GP values were calculated by normalizing poly-GP to BCA levels. N = 6 replicate plates were analyzed. Within-plate replicates of controls were treated separately for the analysis. To eliminate toxic compounds and wells with a detached cell layer during the washing step at harvest, we excluded all replicates with less than 75% mean total protein levels, compared to the solvent controls on each plate. This cut-off eliminated 12 of 708 (1.7%) solvent control measurements, 71 of 528 (13%) individual ASO positive measurements, 142 of 534 (27%) ASO negative control measurements and 1956 of 8844 (22%) other measurements. We selected hits, with at least 3 valid replicates and a minimum of 20% increase or decrease of both absolute and relative poly-GP levels. IC50 for the hit-compounds was determined based on the poly-GP measurements using the Quest Graph™ IC50 Calculator (v.1) (https://www.aatbio.com/tools/ic50-calculator-v1).

Immunofluorescence staining

The cells were fixed in 4% paraformaldehyde (PFA) for 15 min, washed three times with PBS for 5 min each, permeabilized with 0.1% Triton X-100 for 10 min, and washed three times with PBS for 5 min each. Blocking was done with 5% BSA in PBST (PBS + 0.1% Tween 20) for 30 min followed by incubation with diluted primary antibody (in 1% BSA in PBST for iPSC-Neurons and GDB buffer containing 0.1% gelatin, 0.3% Triton X-100, 450 mM NaCl, 16 mM sodium phosphate pH 7.4 for primary rat neurons) in a humidified chamber for 1 h at room temperature or overnight at 4°C: Tuj-1 (1 in 500 dilution, R and D systems, MAB1195), BRN-2 (1 in 1000 dilution, Cell Signaling, 12137), γH2A.X (Ser139) (1 in 250 dilution, Millipore, clone JBW301) and Map2 (1 in 2000 dilution, Millipore, AB5622). After incubation, the cells were washed three times with PBS at room temperature for 5 min each and incubated with appropriate secondary antibodies (conjugated with Alexa Fluor Dyes, Thermo Fisher) in 1% BSA or GDB buffer, respectively, for 1 h at room temperature in the dark. After secondary antibody incubation the cells were washed three times with PBS for 5 min each. The nuclei of iPSC-Neurons were stained with Hoechst 33342 (1 μg/mL) in PBS for 5 min, rinsed once with PBS and imaged. Rat neurons were directly mounted using VECTASHIELD Vibrance Antifade Mounting Medium with DAPI (Vector Labs) and imaged on an inverted Zeiss LSM800 confocal laser scanning microscope (Carl Zeiss) with a 63x oil immersion objective.

Fluorescence *in situ* hybridizations (FISH)

FISH of RNA foci was carried out following the protocol as previously described (Rizzu et al., 2016). Briefly, cells in black, clear bottom 96-well plates (CellCarrier-96, Perkin Elmer) were fixed in 4% PFA for 15 min and washed twice in PBS for 5 min each. After permeabilization with 0.2% Triton in PBS (10 min) and two PBS washes (5 min each), cells were dehydrated twice in 70% ethanol (2 min) and subsequently in 100% ethanol (2 min). Wells were incubated with 100 μL hybridization buffer (10% dextra sulphate, 10 mM Ribonucleoside Vanadyl Complex, 2x Saline Sodium Citrate (SSC) buffer, 50 mM Sodium phosphate buffer pH 7, 50% Formamide in RNAse free water) without probes for 20 min at 66°C. The antisense LNA probes $(CCCCGG)_{2.5}$ (Qiagen product number 339501: Lot: 274175518) and sense LNA probes $(GGGGCC)_{2.5}$ (Lot: 274175516) were diluted at 40 nM in hybridization buffer and denatured at 80°C for 5 min on a heat block, chilled on ice and added to cells after aspirating the pre-hybridization mix. After incubating sealed plates at 66°C for 2 h, they were washed once with 2x SSC/0.1% Tween-20 in RNase-free H_2O for 5 min at room temperature and washed three times using 0.2x SCC buffer in RNase-free H_2O for 10 min each at 65°C. Nuclei were stained with Hoechst 33342 (1 μg/mL) in RNase-free H_2O for 10 min at room temperature followed by a wash step with 0.2x SCC buffer in RNase-free H_2O. The fluorescence images were acquired on an automated microscope (Yokogawa CV7000) at predetermined settings using a water immersion 60x objective and analyzed in batch mode using a predefined pipeline in Columbus (Perkin Elmer). The results are represented as RNA foci load normalized to 100 cells.

To detect RNA foci in *C9orf72* BAC mice, animals were transcardially perfused with PBS. Brains were fixed in 4% PFA, pH 7.4, and embedded in paraffin. 5 μm thick serial sections were cut and mounted onto positively charged microscope slides. After

deparaffinization, FISH of RNA foci was performed as described above with slight modification. Following overnight hybridization at 66°C, slides were washed once with 2x SSC/0.1% Tween-20 in RNase-free H$_2$O for 10 min at room temperature and then washed three times in 0.2x SCC for 10 min at 66°C, 42°C, and 25°C. Autofluorescence of lipofuscin was quenched by 0.3% Sudan Black B in 70% ethanol. Slides were mounted using VECTASHIELD Vibrance Antifade Mounting Medium with DAPI (Vector Labs) and imaged in 10 z-stacks (0.8 μm between stacks) on an inverted Zeiss LSM800 confocal laser scanning microscope (Carl Zeiss) with a 63x oil immersion objective.

Quantitative RT-PCR

If not mentioned otherwise, all qRT-PCR measurements were performed using CFX384 Real Time System (BioRad) and analysis of the data using CFX Manager Software (Version 3.1, Biorad).

iPSC-Neurons

RNA from iPSC-Neurons was isolated using the RNeasy Mini Kit (Qiagen, 74104). RNA integrity (RIN) was determined on the TapeStation (Agilent). Total RNA was primed with oligo-dT (Qiagen) and random decamers (Life Technologies) and was used for cDNA synthesis with Superscript III reverse transcriptase (RT) (Life Technologies) according to manufacturer's specifications. The qPCR was done in triplicates on ViiA7 real time PCR system (Thermo Fisher) using SYBR Green PCR master mix (Thermo Fisher).

Primers for the *C9orf72* transcripts were according to (Waite et al., 2014): *C9orf72* exon 1b (CGGTGGCGAGTGGATATCTC, TGGGCAAAGAGTCGACATCA), *C9orf72* exon 1a (GGGTCTAGCAAGAGCAGGTG, CGACATCACTGCATTCCAAC). As housekeeping genes HMBS (GAAGGATGGGCAACTGTACC, ATGGTAGCCTGCATGGTCTC) and PPIB (CACAGGAGGAAAGAGCATCTAC, CTGTCTTGACTGTCGTGATGAA) were used.

Nascent RNA assay samples

For the measurement of nascent *C9orf72* transcripts the Click-it Nascent RNA Capture Kit (Life Technologies, C10365) was used. After 7 days of differentiation, iPSC-Neurons, were treated with decitabine (10 μM) for a total of 4 days. 24 h prior to harvesting, 0.2 mM 5-ethynyl uridine (EU) was added. Total RNA was isolated using the TRIzol reagent (Invitrogen) following the manufacturer's protocol. Biotinylation of RNA by Click reaction and all the following steps were performed per manufacturer's protocol in the Click-it Nascent RNA Capture Kit using 500 ng of total input RNA for each sample. Reverse transcription for captured RNA was performed using SuperScript™ VILO™ cDNA Synthesis Kit (Thermo Fisher, 11754050). The nascent RNA was analyzed by RT-qPCR using custom IDT PrimeTime qPCR Probe Assays (IDT Gene Expression Master Mix, #1055772). Primer and probes were specifically designed to cover intronic/exon region to detect pre-mRNA of *C9orf72* gene (exon 1a – intron 1) and normalized to TBP (exon 5 – intron 5) pre-mRNA using the ΔΔCT method.

TBP	
forward	CGAACCACGGCACTGAT
reverse	TCATTCATAACCCATAGACCAGAA
probe	AGGAGCCAAGAGGTAGCCGTAAGA
C9orf72	
forward	CCGGTTGCTTCTCTTTTGGGG
reverse	GCGAGTACTGTGAGAGCAAGT
probe	AGGTGTGGGTTTAGGAGGTG

Rat neurons

To measure mRNA in transduced rat neurons, RNA was isolated using the RNeasy Micro Kit (Qiagen, 74004) and M-MLV Reverse Transcriptase (Promega, M1701) following the kit guidelines. qPCR was performed using IDT Primetime qPCR Assays (PrimeTime Gene Expression Master Mix, #1055772). Primers and probes to the tag region of (G$_4$C$_2$)$_n$ construct were designed as described previously (Zhou et al., 2017): Primers TCTCAAACTGGGATGCGTAC and GTAGTCAAGCGTAGTCTGGG, probe TGCAGATATCCAGACAGTGGCG. Signals of repeat constructs derived cDNA were normalized to rat GAPDH (Rn.PT.39a.11180736.g, IDT) according to the ΔΔCT method.

Validation of siRNA in HEK293 cells

To validate the siRNAs, used for treatment of the iPSC-Neurons, HEK cells were seeded in 12-well format and transfected with siRNAs (Silencer Select, Invitrogen) using Lipofectamine RNAiMAX Transfection Reagent (Invitrogen, 13778075) following the manufacturer's protocol. 72 h post transfection with siRNAs cells here harvested and RNA was isolated using the Direct-zol-96 RNA kit (Zymo Research, R2054). cDNA was generated using the High-Capacity RNA-to-cDNA™ Kit (Applied Biosystems, 4387406) and qPCR was performed using the IDT PrimeTime pPCR Assay (PrimeTime Gene Expression Master Mix, #1055772) with GAPDH (Hs.PT.39a.22214836) as housekeeping gene.

Target gene	siRNA 1	siRNA 2	siRNA 3	qPCR assay
C9orf72	s530921	s530920		Hs.PT.58.38350554
MLH1	s297	s224048	s298	Hs.PT.58.40186049.g
MLH2	s10728	s229952	s229951	Hs.PT.58.25954157
MLH3	s534082	s25712	s534081	Hs.PT.58.15434768
MLH4	s10740	s10742	s534926	Hs.PT.58.39275522
MSH2	s534362	s8966	s8967	Hs.PT.58.38933026.g
XRCC6	s5457	s5456	s52594	Hs.PT.58.21136061
FEN1	s5104	s5105	s5103	Hs.PT.58.1554556
XPA	s14926	s14927	s14925	Hs.PT.58.1683980
XPB	s4796	s533737	s4797	Hs.PT.58.15606497
XPC	s14929	s533961	s14928	Hs.PT.58.26563606
negative control	s813			

Mouse samples

RNA isolation from mouse samples was performed as described previously (LaClair et al., 2020) with slight modifications. Tissue was homogenized in RLT-Plus buffer (Qiagen) using a homogenizer (Precellys). Total RNA was isolated using RNeasy Plus Mini Kit (Qiagen). Reverse transcription was performed using random hexamers and TaqMan^{TM} microRNA Kit (Life Technologies) according to manufacturer's instructions. qRT-PCR was performed with IDT PrimeTime qPCR Probe Assays (PrimeTime Gene Expression Master Mix, #1055772). B2m (Assay ID: Mm.PT.39a.22214835) and Actb (Mm.PT.39a.22214843.g) were used as a reference for mouse housekeeping genes. To detect human *C9orf72* isoforms, primers for variants "exon 1a" (Hs.PT.58.1275101) and "exon 1b" (Hs.PT.58.4064580) were selected.

RNAseq

Compound treated iPSC-Neurons were washed with PBS, frozen on dry ice and stored at −80°C until RNA isolation. The RNA was isolated using miRNA Mini Kit (Qiagen) using 700 μL of Qiazol. A total of 250 ng of RNA per sample was processed for mRNA library preparation as per the manufacturer's instructions for Illumina® Stranded mRNA Prep Ligation to be used with the IDT® for Illumina® RNA UD Indexes Set B and sequenced using NextSeq 500/550 High Output Kit v2.5 (Illumina) on NextSeq 550 (Illumina). The data was processed and analyzed using CLC genomics workbench (Version 21.0.3, Qiagen). The average sequencing depth per sample was 37,849,869 reads. The resulting sequences were aligned to the human genome (build hg38) resulting in an average of 98.30% reads mapping to the coding genes and 1.70% reads mapping to the intergenic regions. Pairwise comparisons between the DMSO control and different compound treatments were performed to extract lists of differentially expressed genes using an FDR cut-off (< 0.05).

Analyzing compound binding with surface plasmon resonance (SPR)

5′biotinylated RNA with 10 repeats (Biotin-$(G_4C_2)_{10}$) has been synthesized at Biomers.net GmbH (Ulm, Germany). The RNA was first denatured and then annealed either in 100 mM KCl buffer to form the G-quadruplex (95°C for 5 min, cooling to 5°C in 18 h) or in 100 mM NaCl to adopt hairpin structure (95°C for 5 min, cooling to 25°C in 30 min). The biotinylated RNA was captured using immobilized Neutravidin on a Biacore CM5 chip (capture level 800 RU for hairpin and 2250 RU for G-quadruplex). The compound binding to $(G_4C_2)_{10}$ RNA was measured in a running buffer composed of 10 mM Tris pH 7.4 and 100 mM NaCl (for hairpin) or 100 mM KCl (for G-quadruplex), 0.005% Tween-20, 1% DMSO. At 50 μM the nucleoside analogs showed neglectable binding response to both RNA conformers (below 1 RU) in experiments done by Proteros Biostructures GmbH (Munich, Germany).

Mass spectrometry (MS) analysis

For preparation of DNA and RNA samples for MS analysis, iPSC-Neurons were cultured in 10 cm dishes and treated for the indicated time (1, 4 or 9 days) with decitabine or DMSO. Cells were harvested and pelleted in full media before snap freezing. The frozen cell pellets were used for DNA and RNA isolation (described below). Therefore the cells were disrupted for 2 min at 30 Hz using a TissueLyzer, Qiagen.

Analysis of DNA methylation levels

DNA isolation was performed according to a published protocol (Traube et al., 2019). To inhibit oxidation during the isolation process, all buffers were supplemented with antioxidants 3,5-di-*tert*-butyl-4-hydroxytoluene (BHT, 200 μM) and deferoxamine mesylate salt (Desferal, 200 μM) (Taghizadeh et al., 2008; Traube et al., 2019). The isolated DNA was digested to nucleosides by Nucleoside Digestion Mix (New England BioLabs, M0649S) according to the manufacturer's instructions for 1.5 h at 37°C. Heavy labelled nucleosides were used to spike-in with the final concentration of mdC (10.2 μM), hmdC (0.2 μM), fdC (0.005 μM), cadC (0.004 μM) and 8-oxo-dG

(0.022 μM). All samples were filtered by using an AcroPrep Advance 96 filter plate 0.2 μm Supor (Pall Life Sciences). Solvents for Liquid Chromatography Mass Spectrometry (LC-MS/MS) analysis were purchased from Honeywell, Roth and used without further purification. The analysis was performed using an UHPLC-QQQ-MS/MS system consisting of a Triple Quadrupole 6490 mass spectrometer (Agilent) with an ESI source and an Agilent Infinity 1290 UHPLC. The elution was monitored at 260 nm (Agilent InfinityLab Deuterium Lamp G1314). Data acquisition and processing were performed using MassHunter Workstation Software Version B.07.01 (Agilent). mdC, hmdC, fdC, cadC and 8-oxo-dG were separated on an InfinityLab Poroshell 120 SB-C8 column (2.1 mm × 150 mm, 2.7 μm, Agilent Technologies) at 35°C. Water containing 0.0085% FA (v/v, solvent A) and MeCN containing 0.0085% FA (v/v, solvent B) was used as the mobile phase. A gradient of 0 - 3.5% B for 4 min, 3.5 - 5% B for 2.9 min, 5 - 80% B for 0.3 min, 80% B for 3.3 min was used. The flow rate of the mobile phase was set to 0.35 mL/min. The source-dependent parameters were as follows, gas temperature 80°C, gas flow 15 L/min (N_2), nebulizer 30 psi, sheath gas heater 275°C, sheath gas flow 11 L/min (N_2), capillary voltage 2,500 V in the positive ion mode, and nozzle voltage 500 V. Delta EMV was set to 500 (positive mode). The nucleosides and labelled products were monitored using the multiple reaction monitoring (MRM) mode. The MRM parameters were optimized to achieve maximal detection sensitivity.

Analysis of RNA for incorporation of decitabine

To extract pure RNA samples, the flow-through obtained during the DNA isolation, were purified using Zymo-Spin IIC columns (Zymo Research, C1011) following the manufacturer's protocol and on-column DNA digestion using peqGOLD (peqlab, DNaseI Digest kit). RNA concentration was measured with a NanoPhotometer (Implen, N60, Version NPOS 4.2e build 14900). Based on RNA concentration, the amount of RNA was calculated before digestion to nucleosides by Nucleoside Digestion Mix (New England BioLabs, M0649S) according to the manufacturer's instructions for 1.5 h at 37°C. Before submitting the samples to MS, all samples were filtered through an AcroPrep Advance 96 filter plate 0.2 μm Supor (Pall Life Sciences).

A Dionex Ultimate 3000 HPLC system coupled to a Thermo Fisher LTQ Orbitrap XL mass spectrometer was used for the quantitative HPLC-HESI-MS analysis of the enzymatically digested RNA samples with an injection volume of 45 μL. Nucleosides were separated on an Interchim Uptisphere120-3HDO-C18 column at 30°C. Elution buffers were Buffer A (2 mM NH_4HCOO in H_2O, pH 5.5) and Buffer B (2 mM NH_4HCOO in H_2O/MeCN 20/80 v/v, pH 5.5) with a flow rate of 0.15 mL/min with the following gradient: $0 \to 2$ min, 0% B; $2 \to 20$ min, $0 \to 15$% B; $20 \to 23$ min, $15 \to 85$% B; $23 \to 26$ min, 85% B. The chromatogram was recorded at 260 nm with a Dionex Ultimate 3000 Diode Array Detector and the chromatographic eluent was directly injected into the ion source of the mass spectrometer without prior splitting. Ions were scanned in the positive polarity mode over a full-scan range of m/z 100-1500 with a resolution of 60,000. Further parameters are: Capillary temperature 275°C; source voltage 5.05 kV; vaporizer temperature 100°C, capillary voltage 0 V; tube lens voltage 64 V. The ion chromatograms of the compounds of interest were extracted from the total ion current (TIC) chromatogram, and the areas under the curves were integrated for further calculating of final amounts.

In vitro transcription and translation assay

In vitro transcription and translation assays were performed using the RiboMAX Large Scale RNA Production System-T7 (Promega, P1300) and Flexi Rabbit Reticulocyte Lysate System (Promega, L4540) for transcription and translation reactions, respectively. The plasmid pEF6 (G$_4$C$_2$)$_{80}$ was linearized 3′ of the repeat using PmeI, purified using a column-based PCR purification kit (NucleoSpin Gel and PCR Clean-up, Macherey-Nagel, 740609.250) and used as template in the in vitro transcription reaction with RiboMAX Large Scale RNA Production System-T7. (As a control, Luciferase DNA included in the kit was used). At this step decitabine triphosphate (5-Aza-dCTP, 5-Aza-2′-deoxycytidine-5′-triphosphate, Jena Bioscience, NU-1118) was added additionally to the transcription reaction. While all rNTPs were added at a final concentration of 7.5 mM, different concentrations of 5-Aza-dCTP were used in individual reactions (0, 2, 7.5, 10, 20, 40 mM), both for the repeat containing plasmid as well as for the control plasmid. The reaction was incubated overnight at 37°C. After DNA digestion (37°C, 15 min) using RQ1 RNase-free DNase (Promega, 1 U/μg), the transcribed RNA was purified with RNA Clean & Concentrator-25 kit (Zymo Research, R1017) and concentration was determined using NanoPhotometer (Implen). The quality of the transcribed RNA was controlled performing 2.2 M formaldehyde-2.5% agarose gel electrophoresis using Century-Plus RNA Marker (Ambion, AM7145) as an RNA standard. Therefore, the RNA samples were mixed with Gel Loading Buffer II (Invitrogen, AM8546G) and Formaldehyde (1 μL RNA + 6 μL Loading buffer + 3 μL Formaldehyde) and incubated for 15 min at 65°C and then directly loaded onto the gel. Flexi Rabbit Reticulocyte Lysate System (Promega, L4540) was used for the in vitro translation reaction from 2 μg RNA (overnight at 30°C). DPRs were quantified using the MSD immunoassay as described above.

Cell viability assay

To determine potential toxicity upon treatment of iPSC-Neurons with compounds a LIVE/DEAD staining was performed using LIVE/DEAD^{TM} Viability/Cytotoxicity Kit, for mammalian cells (L3224, Thermo Fisher) following the manufacturer's guidelines using 0.5 μM calcein-AM and 2 μM ethidium homodimer-1. After 30 min incubation at room temperature cells were imaged on an automated microscope (CV7000, Yokogawa Electric Corporation) using 20x objective. The resulting images were analyzed using Cell pathfinder (Yokogawa Electric Corporation) to perform live and dead cells analysis.

Repeat expansion fragment length analysis

The PCR reaction was performed as per manufacturer's guideline using AmplideX® PCR/CE C9orf72 Kit (Asuragen) and run on ABI3130 (Applied Biosystems) for capillary electrophoresis. The fragment sizing analysis was performed in Genemarker 3.0.1 (Softgenetics) to confirm the presence of the expanded *C9orf72* repeat.

siRNA transfection of iPSC-Neurons

Three days after differentiation, iPSC-Neurons (plated in 96-well format) were transfected using Lipofectamine RNAiMax (Thermo Fisher) according to the manufacturer's instructions using 0.17 μL reagent and 0.4 μL siRNA (2.5 μM stock) in 40 μL Opti-MEM I (Thermo Fisher) per well. The next day, the complete media was exchanged to decitabine or DMSO containing media. The compound treatment was repeated on day 9 of differentiation and the cells were harvested 9 days after treatment with decitabine/DMSO and further processed for immunoassay.

QUANTIFICATION AND STATISTICAL ANALYSIS

The statistical details of each experiment are listed in the figure legends, including used statistical tests, exact number of individual biological replicates and precise description of p-values. Statistical significance was determined at a threshold of $p < 0.05$. In case data was not normally distributed according to Shapiro-Wilk test, we used non-parametric tests as indicated. Data was analyzed in R 4.1.2 (Figures 1A–1C, 2C, S2A, S2B, S3B and S3G) or GraphPad Prism 8 (Figures 2A, B, 3A, 3C, 3E, 3F, 4A–4C, S1C–S1E, S2C, S3A, S3C–S3F, S3H, S4A, S4C and S4D). Data are depicted as mean with SEM or SD as indicated in the figure legends. The level of significance is indicated as: ****$p < 0.0001$, ***$p < 0.001$, **$p < 0.01$, *$p < 0.05$.